


BLUFF BODY FLOW

Wake behavior behind a heated circular cylinder

Jan-Jaap Mastenbroek



UNIVERSITY OF TWENTE.
MECHANICAL ENGINEERING
ENGINEERING FLUID DYNAMICS

Acknowledgement

I would like to express my gratitude towards Professor Gustaaf Jacobs, who has given me the opportunity to spend my internship at the San Diego State University, who has supervised me throughout the whole project and who's door was always open for advice.

I would like to thank Prof.Dr.Ir. Harry Hoeijmakers for his support on finding a place for me in the United State to do my internship. Without his help it would not have been possible to find an internship from this quality in this short amount of time.

Thanks to all the lab mates from the Computational Science department, especially Mohammad Abouali, Joris Billen and David Torres. In the 3.5 months they have become good friends, they have given me support during my research and gave me a great insight in the world of science and in the United States.

Thanks to my girlfriend, Emma, my family and friends who have supported me unconditionally throughout the whole internship and made me feel a little bit like home, even at the other side of the world.

Summary

The main objective of this thesis is to get a better understanding of the wake behavior of a circular cylinder when the cylinder is heated. To do so the influence of viscosity on the wake generation is investigated. Results are gained from calculations performed with a DNS CFD program. Also the possibility to manipulate the wake is investigated. The setup is for a case at relatively low speeds, the Reynolds number is set to 200 and the Mach number to 0.2.

As a benchmark, flows with Reynolds numbers varying from 50 - 500 over a non-heated cylinder have been calculated, and the differences are investigated. These differences are then compared to the changes of the wake when the cylinder is heated in the flow at $Re=200$ and $Ma=0.2$. Calculations have been performed for two different fluids, water and air respectively.

With the gained insight a practical setup at the UCLA can be used for a larger variety of flow conditions.

Table of Contents

| | |
|---|----|
| Acknowledgement..... | 1 |
| Summary | 2 |
| List of figures | 4 |
| Chapter 1 - Introduction..... | 5 |
| Motivation | 5 |
| Background on circular cylinder flow | 5 |
| Flow control..... | 10 |
| Outline | 13 |
| Chapter 2 - Computational Method | 15 |
| Governing Equations | 15 |
| Kinematic Viscosity..... | 18 |
| Computational Method..... | 19 |
| Chapter 3 - Results | 22 |
| Benchmark..... | 22 |
| Reynolds number effect | 23 |
| Control of Flow by Heating of Cylinder | 27 |
| Air | 27 |
| Water..... | 30 |
| Case Air - Confirmed..... | 34 |
| Chapter 4 – Conclusions & Recommendations | 37 |
| Conclusions..... | 37 |
| Future Work | 37 |
| Cited Literature..... | 38 |

List of figures

| | |
|---|----|
| Figure 1 - Strouhal's whirling apparatus (1) | 5 |
| Figure 2 - Effect of Reynolds number on wake of circular cylinder (2) | 6 |
| Figure 3 - Strouhal number versus Reynolds number (2) | 6 |
| Figure 4 - Schematically Drawn Transition States (2)..... | 7 |
| Figure 5 - Reynolds number versus Pressure coefficient (4)..... | 9 |
| Figure 6 –Schematic steady wake (4) | 9 |
| Figure 7 - Streamlines influenced by added heat, Air, Re = 40 (10)..... | 11 |
| Figure 8 - Ri versus C_d with different Re (10) | 12 |
| Figure 9 - Angle versus Nu with different Ri, Re 40 (10) | 12 |
| Figure 10 - Trajectories vortices Re=73, Ri=0 (11)..... | 13 |
| Figure 11 - Trajectories vortices Re=73, Ri=1 (11)..... | 13 |
| Figure 12 – Viscosity versus Temperature, Air | 18 |
| Figure 13 – Viscosity versus Temperature, Water | 18 |
| Figure 14 - Physical domain..... | 20 |
| Figure 15 - Used grid | 20 |
| Figure 16 - Zoom of grid | 21 |
| Figure 17 - Development of the Kármán vortex street, Re = 200 | 22 |
| Figure 18 – Re= 200, T=1, Viscosity Constant..... | 23 |
| Figure 19 – Re=200, T=1, Viscosity Constant, Zoom | 23 |
| Figure 20 - Varied Reynolds number | 24 |
| Figure 21 - Average Drag Coefficient versus Reynolds number | 24 |
| Figure 22 – Amplitude of oscillating part of drag versus Reynolds number | 25 |
| Figure 23 - Strouhal number versus Reynolds number | 25 |
| Figure 24 - Time at which wake starts to become oscillating versus Reynolds Number | 26 |
| Figure 25 - Development Kármán vortex street for different cylinder temperatures. Fluid is air, Re=200..... | 27 |
| Figure 26 - Development Kármán vortex street for different cylinder temperatures, Zoom. Fluid is air, Re=200..... | 28 |
| Figure 27 - Drag coefficient versus Time, Varying cylinder temperatures. Fluid is air, Re=200..... | 28 |
| Figure 28 - Average drag coefficient versus Temperature Factor. Fluid is air, Re=200. | 29 |
| Figure 29 - Drag coefficient versus Time for varying cylinder wall temperatures. Fluid is water, Re=200..... | 30 |
| Figure 30 - Drag coefficient versus Time varying cylinder wall temperatures. Fluid is water, Re=200. 31 | |
| Figure 31 - Drag coefficient versus Time, Varying cylinder temperature: Heating. Fluid is water, Re=200..... | 31 |
| Figure 32 - Drag coefficient versus Time, Varying cylinder temperature: Cooling. Fluid is water, Re=200..... | 32 |
| Figure 33 - Average drag coefficient versus Temperature Factor. Fluid is water, Re=200. | 32 |
| Figure 34 – Strouhal number versus Temperature Factor. Fluid is water, Re=200. | 33 |
| Figure 35 – Amplitude of oscillatory part of drag coefficient versus Temperature Factor. Fluid is water, Re=200. | 33 |
| Figure 36 – Streamlines. Temperature factor 1 (left), Temperature factor 1.15 (right). Fluid is air, Re=200..... | 36 |

Chapter 1 - Introduction

Motivation

The goal of this work is to use direct numerical simulation to simulate the behavior of flows around a circular cylinder placed in a parallel flow. This way of simulation quickly provides, accurate and cheap information to research the flow, its behavior and its fluid properties in the neighborhood of the cylinder.

When the model is sufficiently optimized its results can be compared with the results of a physical setup of the same configuration at the University of California, Los Angeles (UCLA). In this way both research methods, numerical and experimental, respectively, can be optimized to provide accurate result of the research field of interest, furthermore insight is gained in the ways to manipulate the flow. Thus really founded conclusions about the behavior and properties of the flow can be gained.

In the next part of this chapter the knowledge of the flow around a bluff body as a research field will be discussed. At the end of this chapter the outline of the research reported in this thesis is given.

Background on circular cylinder flow

The behavior of the flow around a circular cylinder placed in a parallel flow has been subject to significant investigation.

Papers that report work done on the flow over a cylinder in a parallel flow date back to the 19th century. In 1878 it was Strouhal who performed the first scientific experiments on Aeolian tones and published about it in the annals of physics and chemistry (15). These tones are produced when a wire or rod is moved through air. Strouhal did this by attaching the wire between two holders, and then spinning the setup around, see figure 1. In this way the first relation between vortex shedding, in the form of sound, and the Reynolds number was produced.

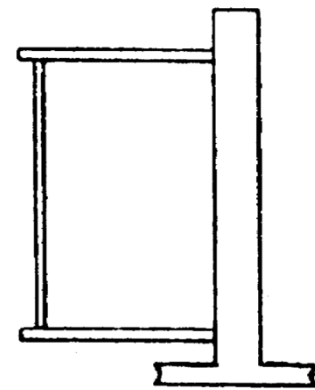


Figure 1 - Strouhal's whirling apparatus (1)

Strouhal concluded that the tension of the wire, its material and the length did not influence the tone produced. Only the speed and the diameter of the rod that influenced the tone. The tone dependency is closely connected to the unsteady, periodic structures that appears in the wake behind a bluff body at Reynolds numbers larger than 50, see figure 2. This is when a so-called Kármán vortex street is formed. A Kármán vortex street is a series of vortex pairs formed at the upper and lower side of a bluff body when a flow with a certain Reynolds number is passing.

The vortex street is formed when the Reynolds number reaches a certain critical value, Re_{cr} , at flows above this Reynolds number the periodic vortex shedding is observed. In the most simple case the Re_{cr} is about 35, with an increasing Reynolds number the wake becomes more complex and for still higher Reynolds numbers will even become turbulent. The Reynolds number is defined as $Re = U_{\infty} d / \nu$, where U_{∞} is the free stream velocity, d is a reference length, in this case the diameter of the circular cylinder, and ν is the kinematic viscosity.

There are several parameters to describe the Kármán vortex street, one of the most important is the Strouhal number, the normalized Strouhal frequency (tones). This value gives the number of vortex pairs that is shedded per unit of time, and is defined as $St = fd/U_\infty$ with f the frequency of the shedding. For different Reynolds numbers come different frequencies of vortex pairs that occur. In figure 3 the Strouhal number is plotted against the Reynolds number for the flow passing a circular cylinder.

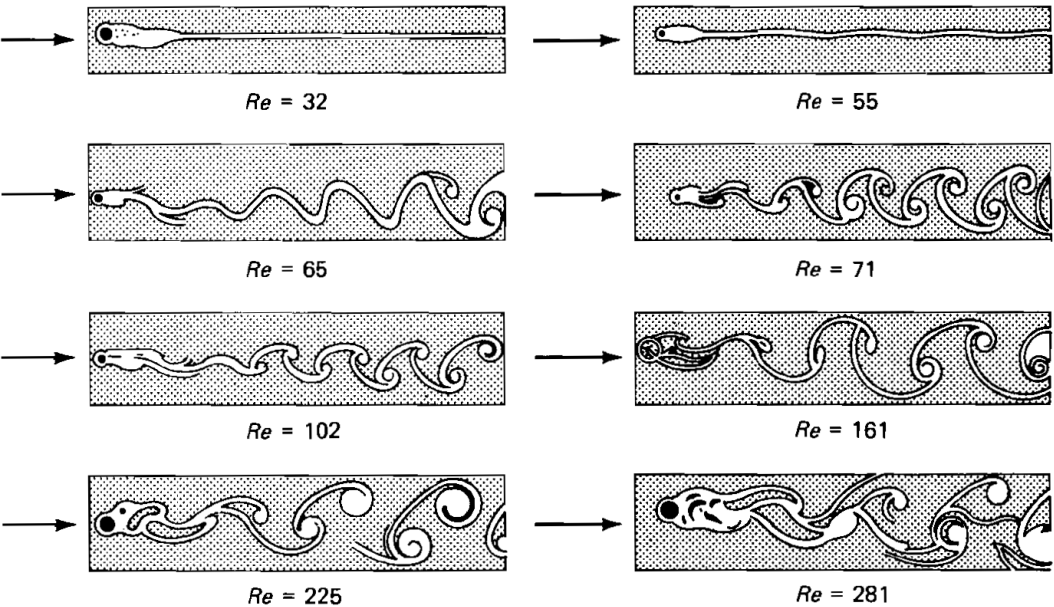


Figure 2 - Effect of Reynolds number on wake of circular cylinder (2)

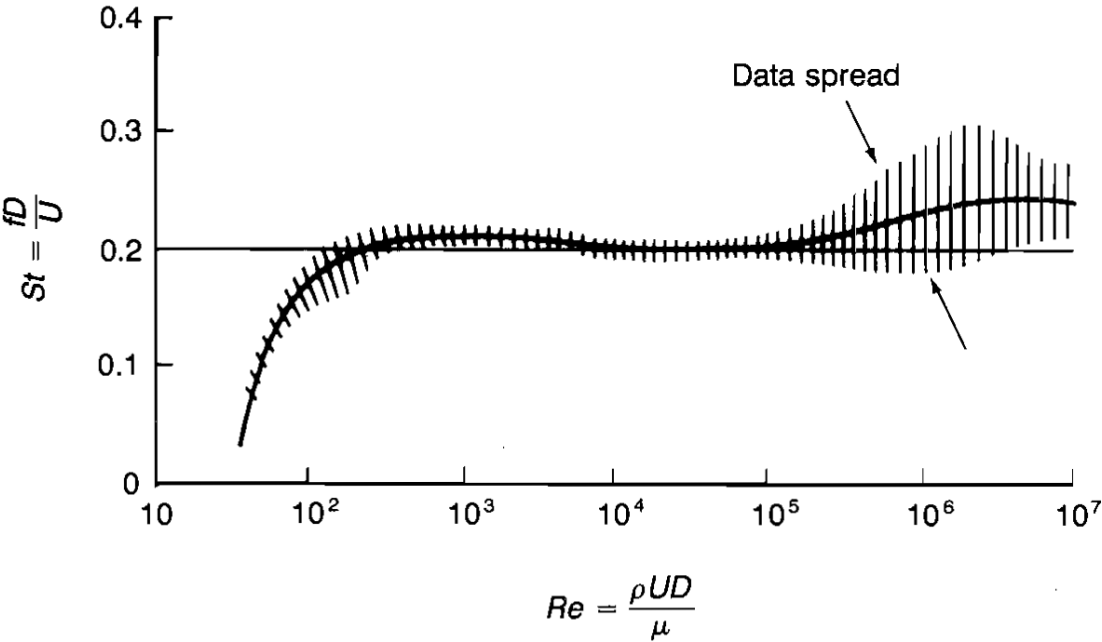


Figure 3 - Strouhal number versus Reynolds number (2)

With increasing Reynolds number the Kármán street experiences a number of bifurcations. The behavior of the Kármán street may also be affected actively, i.e. by changing the temperature of the cylinder, oscillating the cylinder or changing its roughness. In most of the cases these changes result in an effective Reynolds number different than the Reynolds number itself.

Forms

The characterization of the flow over a cylinder, and bluff bodies in general, is rather complicated since there are three shear layers involved that interact with each other; a boundary layer, a separating free shear layer and a wake (1). There have been several attempts to identify parameters that uniquely characterize bifurcations in the wake’s behavior. Here, we will discuss approaches Zdravkovich (1) and Williamson (4) have suggested.

Zdravkovich - The wake, going from fully laminar (L) to fully turbulent (T), is described by four transition states, as shown in figure 4. The first transition flow, figure 4 (a), is observed when laminar vortices in the wake become turbulent due to 3D distortions downstream of the cylinder. The higher the Reynolds number, the more upstream the transition region will appear. The free shear layers remain laminar.

The second transition state (b) is the state in which the free shear layers get turbulent. The third transition state (c) is “an extremely complicated interaction between the separation and transition before the boundary layers become fully turbulent along the separation line.”. In the last transition state the shear layers upstream of the separation points get turbulent, with increasing Reynolds numbers even up to the stagnation point. After this transition state all regions further downstream are fully turbulent.

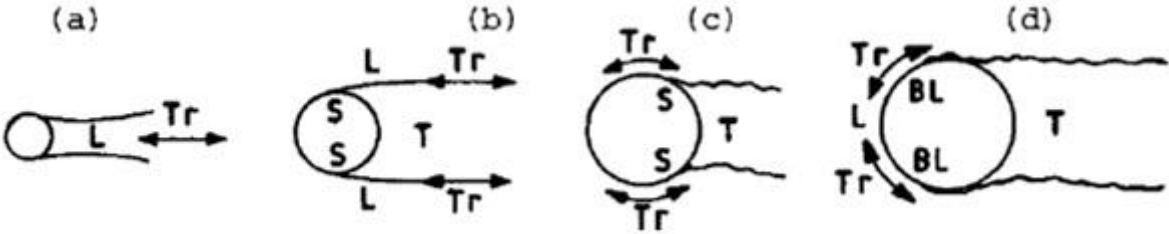


Figure 4 - Schematically Drawn Transition States (2)

It is important which Reynolds numbers are involved with which transition state. The transition states are again subdivided, and the results are given in table 1.

| State of Flow | Name | Description | Reynolds Regime |
|---|-------|---|--------------------------------------|
| Laminar | L1 | 'creeping' flow (no-separation) | $0 < Re < 4$ to 5 |
| | L2 | steady separated flow region (closed near-wake) | 4 to $5 < Re < 30$ to 48 |
| | L3 | periodic laminar wake | 30 to $40 < Re < 150$ to 200 |
| Transition in wake | TrW1 | transition of laminar vortices in wake | 150 to $200 < Re < 200$ to 250 |
| | TrW2 | transition of vortices during formation | 200 to $250 < Re < 350$ to 500 |
| Transition in free shear layers | TrSl1 | transition waves in free shear layers | 350 to $500 < Re < 1k$ to 2k |
| | TrSl2 | transition vortices in free shear layers | $1k$ to $2k < Re < 20k$ to 40k |
| | TrSl3 | fully turbulent shear layers | $20k$ to $40k < Re < 100k$ to 200k |
| Transition around separation of boundary layer | TrS0 | onset of transition of separation | $100k$ to $200k < Re < 320k$ to 340k |
| | TrS1 | single separation bubble regime | $320k$ to $340k < Re < 380k$ to 400k |
| | TrS2 | two-bubble regime | $380k$ to $400k < Re < 500k$ to 1M |
| | TrS3 | supercritical regime | $500k$ to $1M < Re < 3.5M$ to 6M |
| Transition in boundary layers | TrBL | transcritical regime | $3.5M$ to $6 < Re < 6M$ to 8M |
| Turbulent boundary layers | | postcritical regime | $Re > 8M$ |
| | | ultimate regime | $Re \rightarrow \infty$ |

Table 1 - Classification of disturbance free flow regime (1)

Williamson - Another way to categorize the flow regimes and the transition regimes is through the base suction coefficient ($-C_{pb}$). This coefficient represents the dimensionless pressure at the point 180 degrees from front the stagnation point. The plot in figure 5 presents this coefficient against the Reynolds number. This is useful because the different flow regimes can be easily distinguished. It appears that the base suction coefficient is “sensitive to the process of vortex formation in the near wake, which itself is affected strongly by the evolution of various 2D- and 3D wake instabilities, as the Reynolds number is varied.” (4)

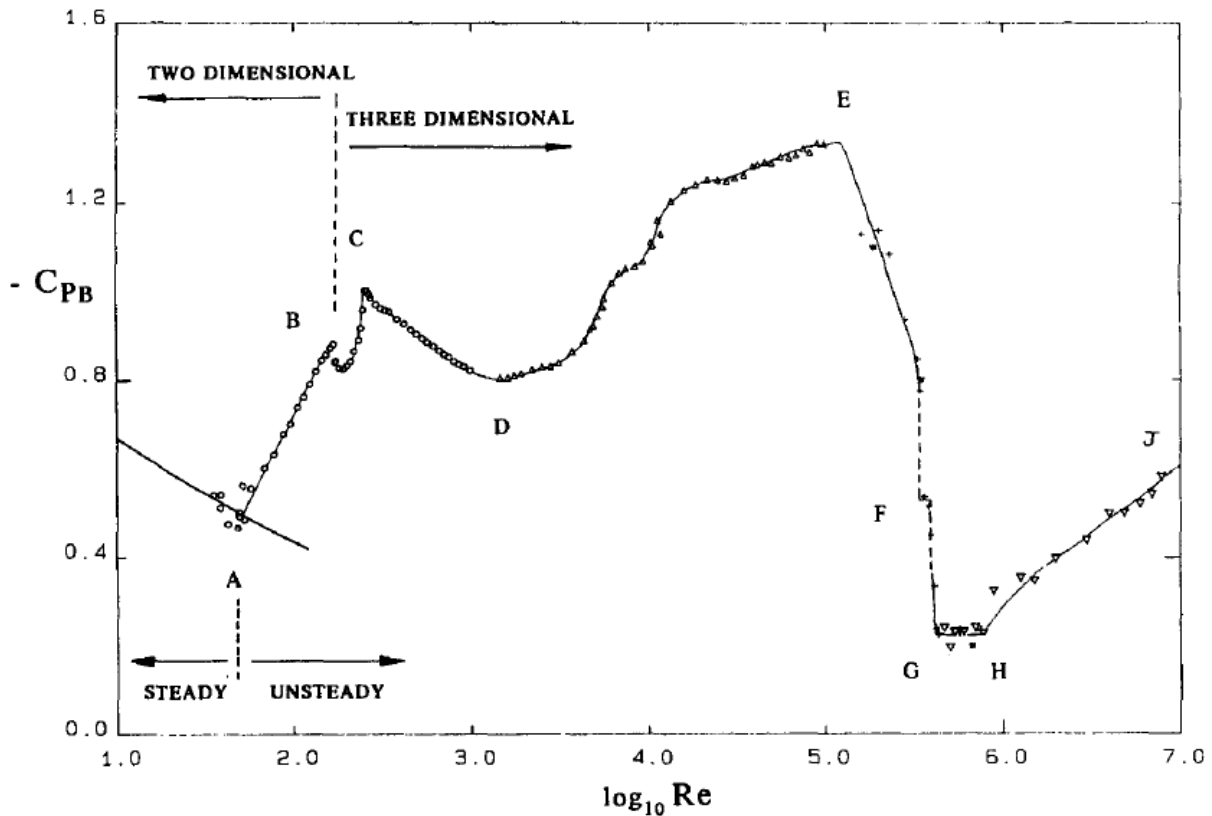
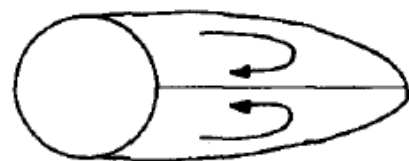


Figure 5 - Reynolds number versus Pressure coefficient (4)

In figure 5 there are 9 different regions which specify different flows and transitions.

- Up to point A the wake consists of a steady and symmetric flow with two stationary vortices behind the cylinder, as shown in figure 6. The higher the Reynolds number becomes, the longer the vortical flow regime will be.
- The region from A to B, is characterized by the beginning of vortex shedding. The oscillations in this regime are periodic.
- The regime from B to C is the 3D wake transition regime. In this regime there are two discontinuous changes in the wake formation. The first discontinuity ($Re = 180-194$) is caused by vortex loop inception, this discontinuity is hysteretic, so different $-C_{pb}$ values are possible at the same Reynolds number. The differences depend on the way the data is gained, whether the flow speed is increased or decreased to reach the Reynolds number in this regime. The second discontinuity ($Re = 230 - 250$) the shedding mode changes due to 3D effects.
- From regime C to D there is an increasing disorder in the fine-scale 3D effects. Although there are 3D effects, and the 2D dominant stresses decrease with increasing Reynolds number, the instabilities act more or less like they are laminar, up to $Re = 1000$.



STEADY WAKE

Figure 6 –Schematic steady wake (4)

- The region from D up to E is called the Shear layer transition regime. In this regime the increasing instability that appears in the wake is caused by the separating shear layer from the sides of the cylinder.
- The regime from E to G is the asymmetric reattachment regime, or critical regime, here the boundary layer separates further downstream. Further regimes are not of interest and beyond the scope of the research.

Table 2 gives the different regimes with their Reynolds numbers.

| Graph | Description | Reynolds regime |
|---------|--|---------------------|
| Up to A | Laminar Steady Regime | $Re < 49$ |
| A to B | Laminar Vortex Shedding Regime | $49 < Re < 140-194$ |
| B to C | 3-D Wake-Transition Regime | $160 < Re < 260$ |
| C to D | Increasing Disorder in the Fine-Scale Three Dimensionalities | $260 < Re < 1000$ |
| D to E | Shear-Layer Transition Regime | $1k < Re < 200k$ |
| E to G | Asymmetric Reattachment Regime | $200k < Re < 500k$ |
| G to H | Symmetric Reattachment Regime | $500k < Re < 1M$ |
| H to I | Boundary-Layer Transition Regime | $1M < Re$ |

Table 2 - Flow regimes by Williamson (4)

Despite the different methods of identifying the flow and transition regimes the results, Reynolds numbers at which the flow changes, of (1) and (4) match very well. Only small differences appear, such as the slightly different Reynolds number at which the shedding starts.

Overall it can be concluded that the shedding starts at a Reynolds number of 35 – 49, the wake is 2D up to a Reynolds number of 200, and that the wake becomes really complicated after Reynolds numbers of 1000.

Flow control

There are several ways in which one may control the Kármán wake. It even can be suppressed, or provoked.

Heating the cylinder at low Reynolds numbers, has significant influence on the forming of the Kármán street. The heating affects the properties as density, viscosity and thermal conductivity of the fluid. This alters the characteristics of the vortex shedding (5).

| Reynolds Number | ΔC° | $Re_{\text{effective}}$ |
|-----------------|------------------|-------------------------|
| 48.1 | 28.2 | 46.1 |
| 50.1 | 63.8 | 46.1 |
| 52.1 | 90.2 | 46.1 |
| 54.1 | 114.1 | 46.1 |
| 55.8 | 145.9 | 46.1 |

Table 3 - Effect of heating on $Re_{\text{effective}}$, Air (5)

Table 3 shows an example that heating the cylinder results in a lower effective Reynolds number and that thus the wake, the Kármán street, is affected. In this low Reynolds number case, in which the fluid is air, it is even possible to totally suppress the vortex shedding. At a higher Reynolds number, more heat input is required to suppress the shedding. Though suppressing the Kármán street is

limited to low Reynolds numbers, i.e. $Re = 45-120$ (12). At higher Reynolds numbers the amount of heat needed for suppression will induce other influences that will become predominant.

The opposite behavior is found when the fluid is water. When a heated cylinder is put in a flow of water the effective Reynolds number will be higher than the actual Reynolds number. Thus the Kármán street will form at a lower Reynolds number.

In figure 7 the stimulation and suppression of the vortex street are visualized for a Richardson number of -1.0 and $+1.0$ respectively at a Reynolds number of 40 in a flow of air. The added heat is described with this dimensionless Richardson number, defined as $Ri = Gr / Re^2$. The Richardson number is chosen -1.0 for cooling, up to $+1.0$ for heating. When the Richardson number is 0 no heat is added.

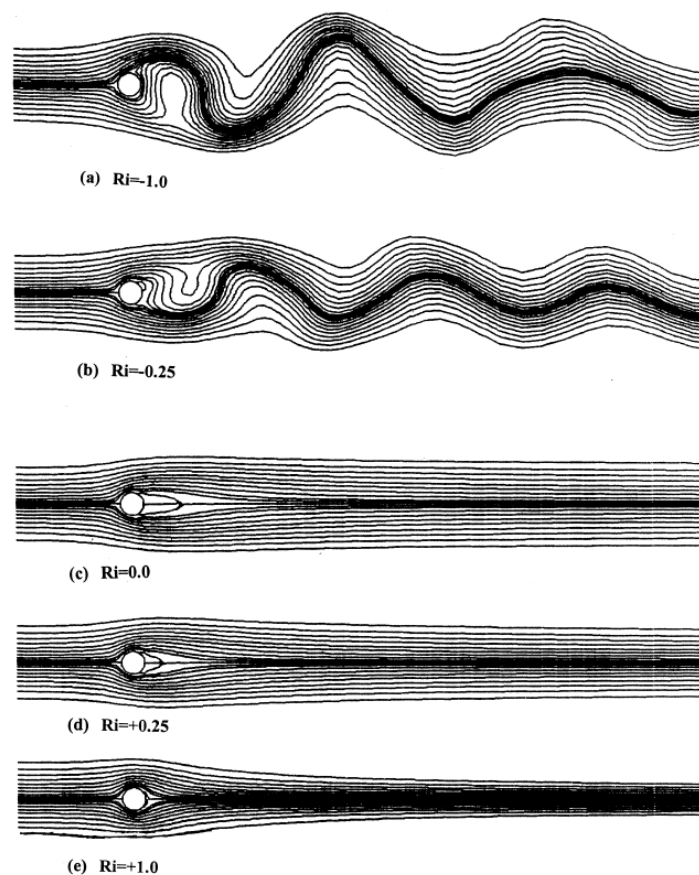


Figure 7 - Streamlines influenced by added heat, Air, $Re = 40$ (10)

The causes of this difference in behavior is still a point of discussion. Sometimes the effect is related to *"...the increase of the kinematic viscosity of the gas and to the corresponding decrease of the effective Reynolds number..."* (7). Others argue that the effect is caused by density changes in the near wake (8). And there is literature that reports that the effect is due to changes with temperature of both the near wake dynamic viscosity and density (9).

When the heat input of the cylinder becomes too high, buoyancy effects will affect the wake behavior, especially when the fluid is water. Buoyancy effects can be predominant to the variable

fluid properties. A lot of research has been done on the consequences of the buoyancy effect. These effects appear only at low Reynolds number though.

Other interesting results are reported by Varaprasad (10), shown in figure 8 and figure 9. As can be seen in figure 8, at relative high Reynolds numbers the drag coefficient is not seriously affected by heating when compared to the lower Reynolds number cases, here the drag coefficient increases when the added heat is increased, at these low Reynolds numbers buoyancy effect play an important role.

The variation in the Nusselt number ($Nu=0-8$) for different Richardson numbers, again points out that the buoyancy effect does play a role at very low Reynolds numbers. This is shown in figure 9.

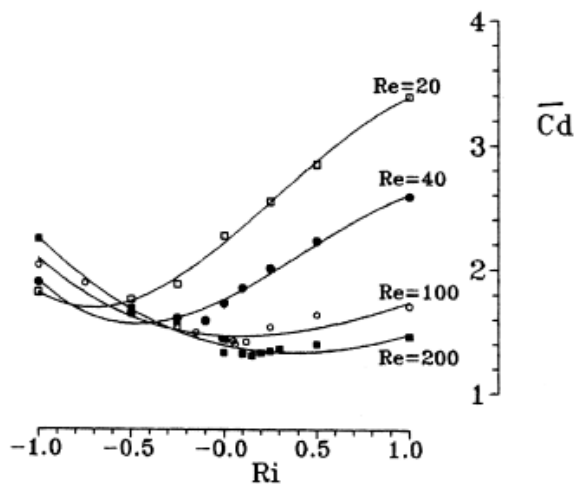


Figure 8 - Ri versus C_d with different Re (10)

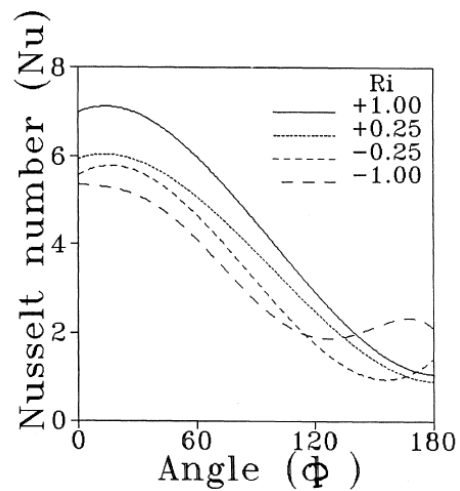


Figure 9 - Angle versus Nu with different Ri, Re 40 (10)

The wake behavior

The behavior of the wake behind a horizontal heated circular cylinder at low Reynolds numbers has been investigated experimentally many times. An example is the work of Kieft et al. (11). Here the Reynolds number is 73, and the Ri number is varied between 0 and 1. Kieft assumed all fluid properties to be constant, thus not to be affected by the temperature difference because they are small. Only the buoyancy effects are taken into account. Results of his research are shown in figures 9 and 10.

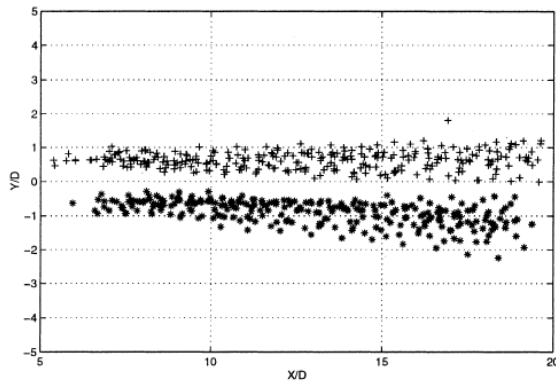


Figure 10 - Trajectories vortices $Re=73$, $Ri=0$ (11)

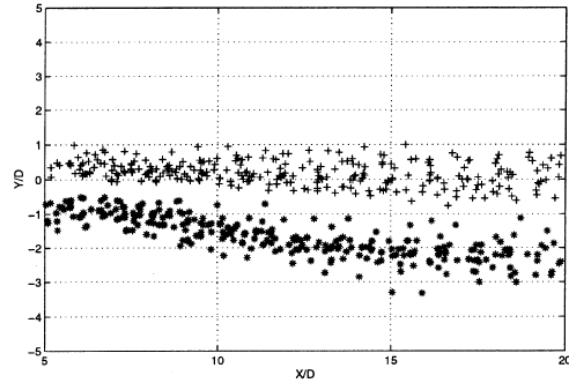


Figure 11 - Trajectories vortices $Re=73$, $Ri=1$ (11)

The graphs clearly show a downward movement of the lower vortex row. This behavior is unexpected because the movement is opposite to the forces induced by the buoyancy effect. Kieft explains the movement from the differences in strength between the upper and lower vortices from vorticity produced due to density variations.

Outline

As made clear it is still a point of discussion what exactly causes the changes in the Kármán street when heat is added to the cylinder. Some relate the effect to the in-/decrease of kinematic viscosity, others to a combination of the changing viscosity and changing density, and others take buoyancy effects into account as well.

In this thesis we investigate influence of the fluid's viscosity on the flow and wake. Also the possibility to manipulate the wake behind a cylinder by changing the temperature of this cylinder is investigated. The setup is for a case at relatively low speeds, the Reynolds number is set to 200 and the Mach number to 0.2.

The viscosity is programmed to be temperature dependent. For air the Sutherland's law (2) is used to describe the relationship of the viscosity with temperature. Because these relationships of the viscosity with temperature of water and air are different, we expect a different behavior for these cases. The temperature of the cylinder is changed relative to the surrounding flow with factors from 0.85, i.e. cooled 15%, to 1.4, i.e. heated by 40%. The calculations are performed with a DNS CFD program.

In this research the influences of the buoyancy effect are assumed to be negligible. The speed of the flow is too high for the buoyancy effects to play a role of interest (10). The effect of heating on density is the same for water and air, they both decrease.

Thus the parameter that is changed during the research is the temperature, the fluid property that changes with it, is the viscosity. Although there is only one fluid property subject to change, the flow is a good representation of the real flow, because all the other property changes are assumed to be negligible.

The results of this research will provide insight in the behavior of the flow and the influence of the viscosity when heat is added or subtracted. The results can be compared with the results of the physical setup, the results can be used to optimize the physical setup and to get a better insight in the behavior of the real flow. Furthermore a better understanding of flow manipulation is gained.

In chapter 2 we discuss the used CFD program and governing equations including Sutherland's law for viscosity dependency on temperature. In Chapter 3 we present and discuss the results. The conclusions and recommendations are presented in chapter 4.

Chapter 2 - Computational Method

Governing Equations

In this paragraph the governing equations used by the CFD method are presented. The used equations are dimensionless to prevent possible effects generated by the disparity of physical variables (13).

Before summing the equations, the following assumptions concerning these equations are made:

- The fluid is continuous, i.e. the smallest length scales occurring in the motion of the fluid flow are very large compared to the mean free path of the molecular motion.
- The heat flux in the energy equation obeys Fourier's law.
- The fluid is an ideal gas, for which intermolecular forces are negligible, and obeys the equation of state $p = \rho RT$, where R is the gas constant.

The physical variables are non-dimensionalized by a reference length L_f^* , density ρ_f^* , velocity U_f^* , temperature T_f^* and viscosity μ_0^* . The superscript * denotes a dimensional variable. This gives the following non-dimensionalization of the variables:

$$\begin{aligned} \rho &= \rho^* / \rho_f^* & p &= p^* / (\rho_f^* U_f^{*2}) \\ u &= u^* / U_f^* & x &= x^* / L_f^* \\ v &= v^* / U_f^* & y &= y^* / L_f^* \\ w &= w^* / U_f^* & z &= z^* / L_f^* \\ T &= T^* / T_f^* & t &= t^* U_f^* / L_f^* \\ \mu &= \mu^* / \mu_0^* \end{aligned}$$

The dimensionless equations for mass, momentum and energy, or the Navier Stokes equations, in conservation form and Cartesian coordinates are given by:

$$\vec{Q}_i + \vec{F}_x^a + \vec{G}_y^a + \vec{H}_z^a = \frac{1}{\text{Re}_f} (\vec{F}_x^v + \vec{G}_y^v + \vec{H}_z^v)$$

Where the arrows represent vectors, and

$$\vec{Q} = \begin{bmatrix} \rho \\ \rho u \\ \rho v \\ \rho w \\ \rho e \end{bmatrix}, \vec{F}^a = \begin{bmatrix} \rho u \\ p + \rho u^2 \\ \rho uv \\ \rho uw \\ u(\rho e + p) \end{bmatrix}, \vec{G}^a = \begin{bmatrix} \rho v \\ \rho uv \\ p + \rho v^2 \\ \rho vw \\ v(\rho e + p) \end{bmatrix}, \vec{H}^a = \begin{bmatrix} \rho w \\ \rho uw \\ \rho vw \\ p + \rho w^2 \\ w(\rho e + p) \end{bmatrix}$$

And

$$\vec{F}^v = \begin{bmatrix} 0 \\ \tau_{11} \\ \tau_{12} \\ \tau_{13} \\ u\tau_{11} + v\tau_{12} + w\tau_{13} + \frac{1}{(\gamma-1)M_f^2 \text{Pr}} T_x \end{bmatrix}$$

$$\vec{G}^v = \begin{bmatrix} 0 \\ \tau_{21} \\ \tau_{22} \\ \tau_{23} \\ u\tau_{21} + v\tau_{22} + w\tau_{23} + \frac{1}{(\gamma-1)M_f^2 \text{Pr}} T_y \end{bmatrix}$$

$$\vec{H}^v = \begin{bmatrix} 0 \\ \tau_{31} \\ \tau_{32} \\ \tau_{33} \\ u\tau_{31} + v\tau_{32} + w\tau_{33} + \frac{1}{(\gamma-1)M_f^2 \text{Pr}} T_z \end{bmatrix}$$

Where,

$$\begin{aligned} \tau_{11} &= 2\mu \left[u_x - (u_x + v_y + w_z)/3 \right], \\ \tau_{22} &= 2\mu \left[v_y - (u_x + v_y + w_z)/3 \right], \\ \tau_{33} &= 2\mu \left[w_z - (u_x + v_y + w_z)/3 \right], \\ \tau_{12} &= \tau_{21} = \mu \left[v_x + u_y \right], \\ \tau_{13} &= \tau_{31} = \mu \left[w_x + u_z \right], \\ \tau_{23} &= \tau_{32} = \mu \left[w_y + v_z \right], \\ \rho e &= \frac{P}{\gamma-1} + \rho(u^2 + v^2 + w^2)/2 \end{aligned}$$

In above equations the superscript 'a' denotes inviscid fluxes, these are the same as the corresponding terms in the dimensional equations. The superscript 'v' denotes the viscous fluxes, these fluxes give rise to the following non-dimensional parameters:

- The reference Reynolds number, which indicates the influence of the viscous fluxes as compared to the advective fluxes, defined as $Re_f = U_f^* L_f^* \rho_f^* / \mu^*$.
- The Prandtl number, which is the ratio of the viscous and thermal diffusivity, defined as $Pr = c_p^* \mu^* / \kappa^*$, where c_p^* is the specific heat at constant pressure of the fluid.
- The reference Mach number, $M_f = U_f^* / c^*$, where c^* is the reference speed of sound defined as $c^* = \sqrt{\gamma R^* T_f^*}$, and $\gamma = c_p / c_v$.
- The viscosity μ is dependent on the temperature, the relation are given below.

The ideal gas equation of state in non-dimensional form is given by

$$p = \frac{\rho T}{\gamma M_f^2}$$

The original Sutherland law is adjusted for the performed calculations. The implemented codes for the viscosity dependency on temperature for air and water are:

$$\mu(T) = \frac{\mu_0}{\mu_{ref}} \left(\frac{T_{ref} T}{T_0} \right)^{3/2} \left(\frac{T_0 + S}{T \cdot T_{ref} + S} \right)$$

with

$$\mu_0 = 1.716 \cdot 10^{-5} \text{ kg / m} \cdot \text{s}$$

$$\mu_{ref} = 1.5995 \cdot 10^{-5} \text{ kg / m} \cdot \text{s}$$

$$T_0 = 273K$$

$$T_{ref} = 10K$$

$$S = 111K$$

Implemented code for Air

$$\mu(T) = \frac{\mu_0}{\mu_{ref}} \exp \left(a + b \left(\frac{T_0}{T_{ref} \cdot T} \right) + c \left(\frac{T_0}{T_{ref} \cdot T} \right)^2 \right)$$

with

$$\mu_0 = 0.00179 \text{ kg / m} \cdot \text{s}$$

$$\mu_{ref} = 8.6656 \cdot 10^{-4} \text{ kg / m} \cdot \text{s}$$

$$T_0 = 273K$$

$$T_{ref} = 12K$$

$$a = -2.10$$

$$b = -4.45$$

$$c = 6.55$$

Implemented code for Water

Kinematic Viscosity

As outlined in chapter 1, the behavior of Kármán streets behind a heated cylinder at low Reynolds numbers in water and air is different. In air, the street can be suppressed with heating, in water the street will be provoked by heating the cylinder. The same kind of trend can be found in the change of kinematic viscosity with temperature. As can be seen in figure 12 the viscosity of air increases with increasing temperature whereas the viscosity of water decreases with increasing temperature, see figure 13.

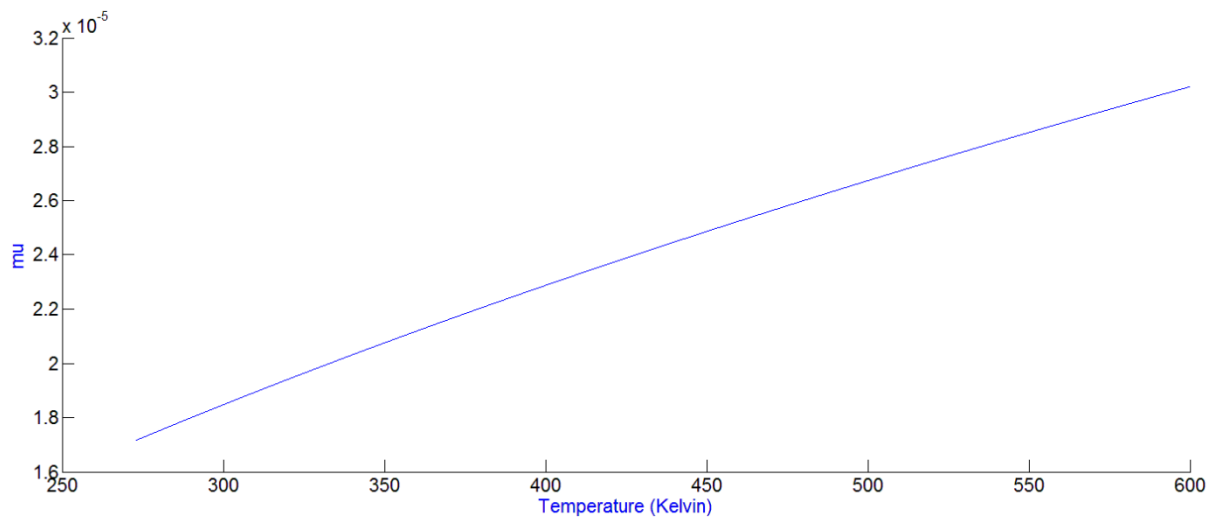


Figure 12 – Viscosity versus Temperature, Air

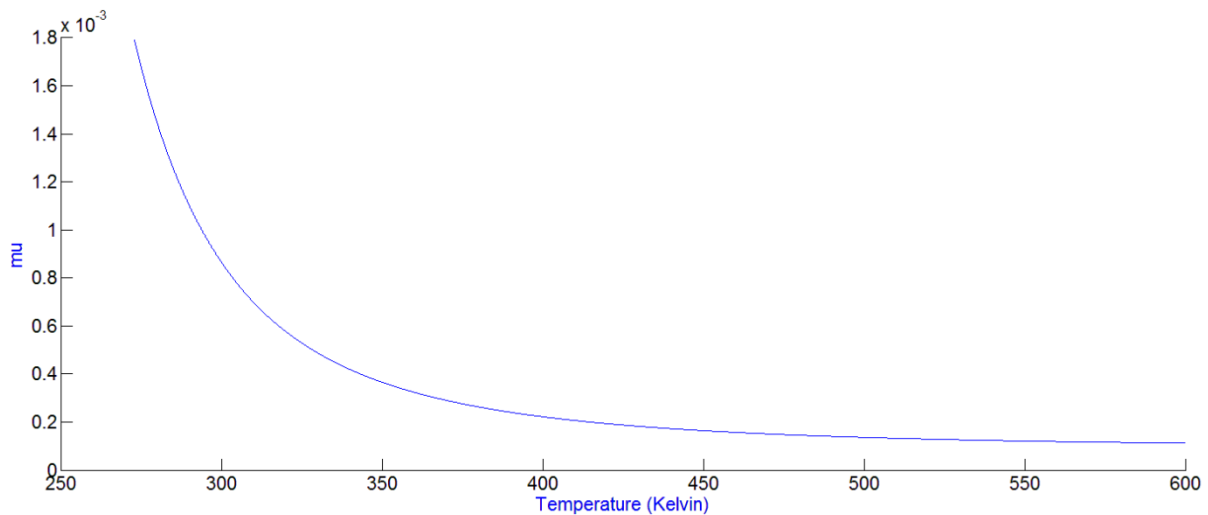


Figure 13 – Viscosity versus Temperature, Water

Figures 12 and 13 are graphical representations of the relation between temperature and viscosity as implemented in the CFD code. For air and water the laws are respectively:

$$\mu = \mu_0 \left(\frac{T}{T_0} \right)^{3/2} \left(\frac{T_0 + S}{T + S} \right)$$

With:

$$\mu_0 = 1.716 \cdot 10^{-5} \text{ kg / m} \cdot \text{s}$$

$$T_0 = 273 \text{ K}$$

$$S = 111 \text{ K}$$

And for water

$$\mu \approx \mu_0 \exp \left(a + b \left(\frac{T_0}{T} \right) + c \left(\frac{T_0}{T} \right)^2 \right)$$

With:

$$\mu_0 = 0.00179 \text{ kg / m} \cdot \text{s}$$

$$T_0 = 273 \text{ K}$$

$$a = -2.10$$

$$b = -4.45$$

$$c = 6.55$$

The CFD program that is used for simulating the flow is based on a staggered-grid Chebyshev multidomain method for the solution of compressible flow problems. For details of the code and used methods see the work of Jacobs (13) or for further details see Kopriva's work (14).

Computational Method

The physical domain is shown in figure 14. The cylinder diameter is defined as L and its center is located in the middle of the domain. The inflow region, left side, is placed 19.5 (a) diameters in front of the cylinder, the main outflow region, right, is placed 49.5 (c) diameters behind the cylinder. The upper and lower borders are placed 19.5 (b) diameters above and under the cylinder, this is sufficiently far away to assume probable blockage does not affect the flow. The thick boundaries surrounding the cylinder are inflow/outflow boundaries.

At the inlet the inflow is uniform and homogeneous. On the cylinder the no slip conditions are prescribed, $u=0$ and $v=0$. The temperature of the cylinder is uniform.

The following non dimensional values are used and prescribed:

$$u = 1$$

$$\rho = 1$$

$$Ma = \frac{u}{\sqrt{T}}$$

$$T = 10$$

$$p = \frac{\rho T}{\gamma}$$

$$Re = \frac{uL}{\nu}$$

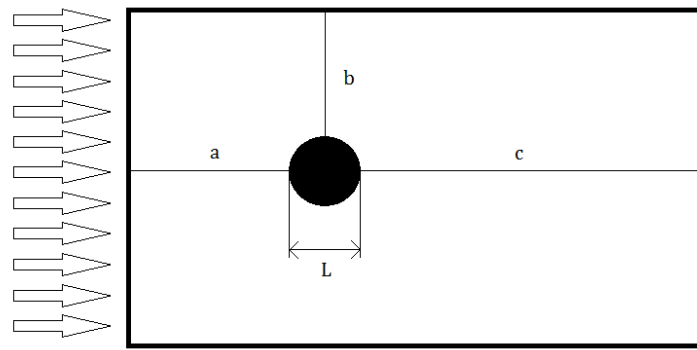


Figure 14 - Physical domain

In figure 15 the grid is shown that is used for the CFD calculations. The grid is refined around the cylinder and in its wake, as can be seen in figure 16, it is more coarse away from the cylinder. A convergence study has proven that the used grid is accurate and reliable. The study is performed by Jacobs, for further details see his work (13).

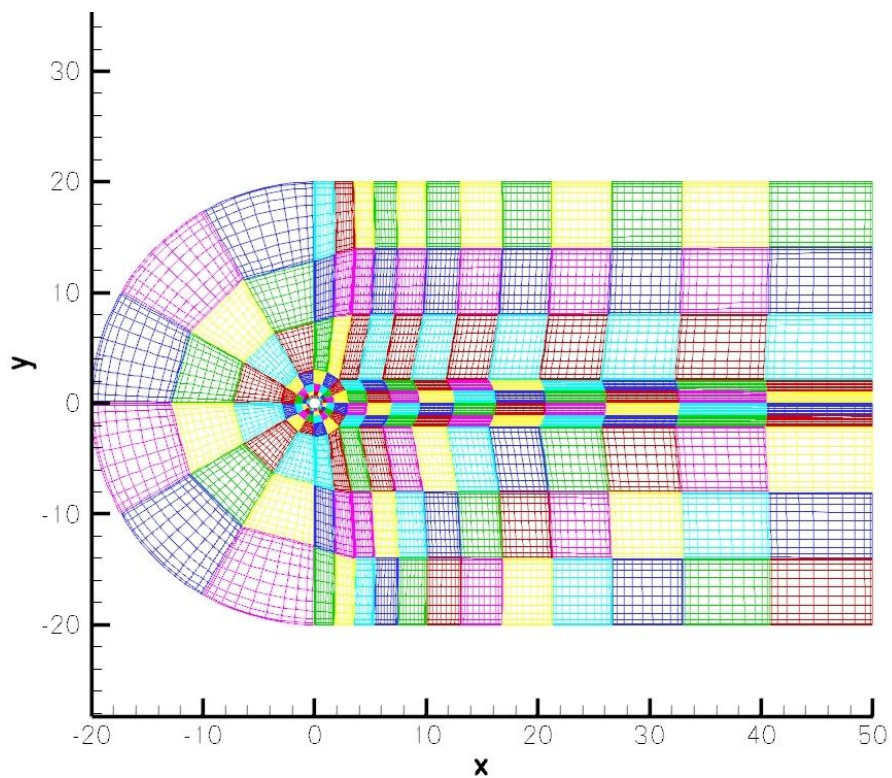


Figure 15 - Used grid

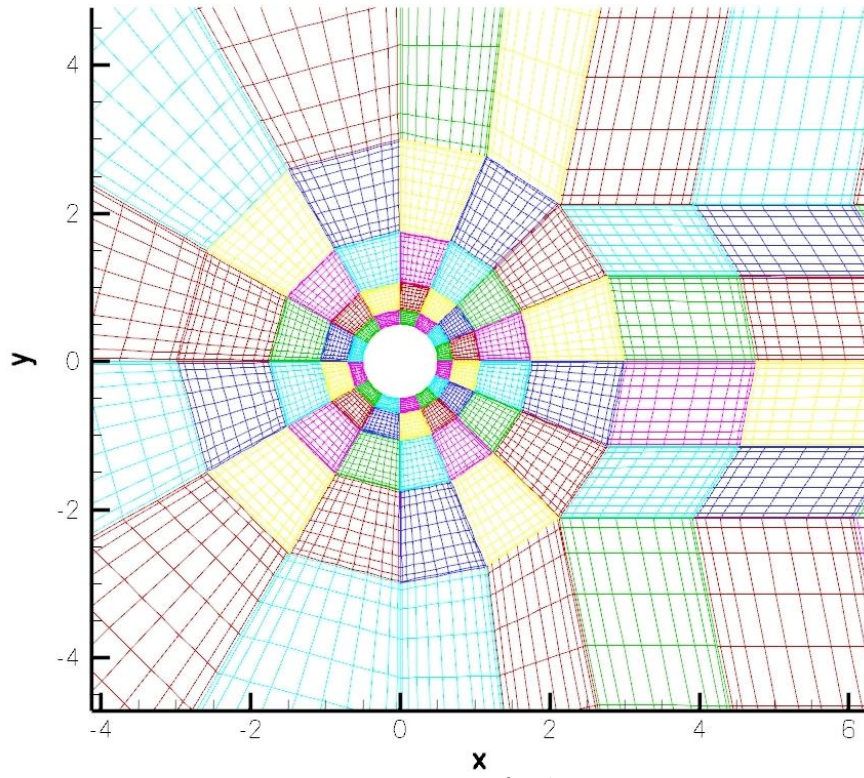


Figure 16 - Zoom of grid

Chapter 3 - Results

Benchmark

We discuss the flow over a cylinder at a Reynolds number of 200 and a Mach number of 0.2 as a reference.

Figure 17 shows the wake for different times to give an insight in the development of the street. The wake is shown at different time steps, from left to right, 10, 30, 130, 145, 150 and 201 respectively. The first two snapshots both show a still laminar, symmetric and stable wake, the only difference in time is the length of the wake. The region of the flow that is affected by the presence of the cylinder gets bigger with time. After 130 time steps, snapshot 3, the wake is disturbed abruptly and becomes turbulent. It takes until timestep 200 before the turbulent flow to fully develop. After 200 timesteps, snapshot 6, the wake is developed and the flow pattern repeats itself, i.e. is periodic.

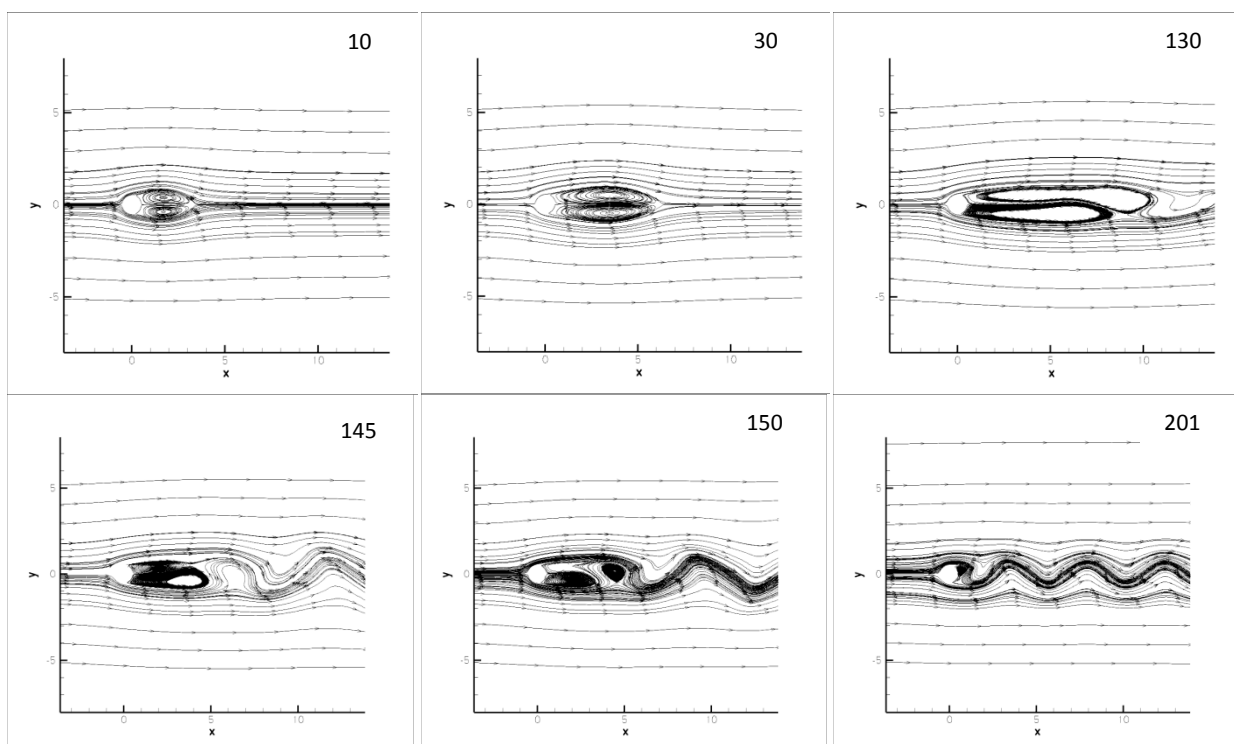


Figure 17 - Development of the Kármán vortex street, $Re = 200$

In figure 18 the drag coefficient of the cylinder is plotted against the time steps. The figure shows the change in drag experienced by the cylinder. The shedding of a vortex induces large changes in the drag, thus the variation of the drag coefficient gives a perfect insight in the vortex shedding and thus the, development of, the Kármán vortex street. The drag coefficient as calculated by the CFD code is only based on the surface pressure, it is not a combination of the pressure and wall friction drag. The same method is use by Williamson (4).

At the start of the flow the drag coefficient gives extreme values, these are caused by the startup phase. From timestep 0 until approximately timestep 130 the flow is stable and symmetrical. It takes the street from time step 130 until approximately time step 200 to fully develop. After time step 200 the street is fully developed and oscillating at a constant rate.

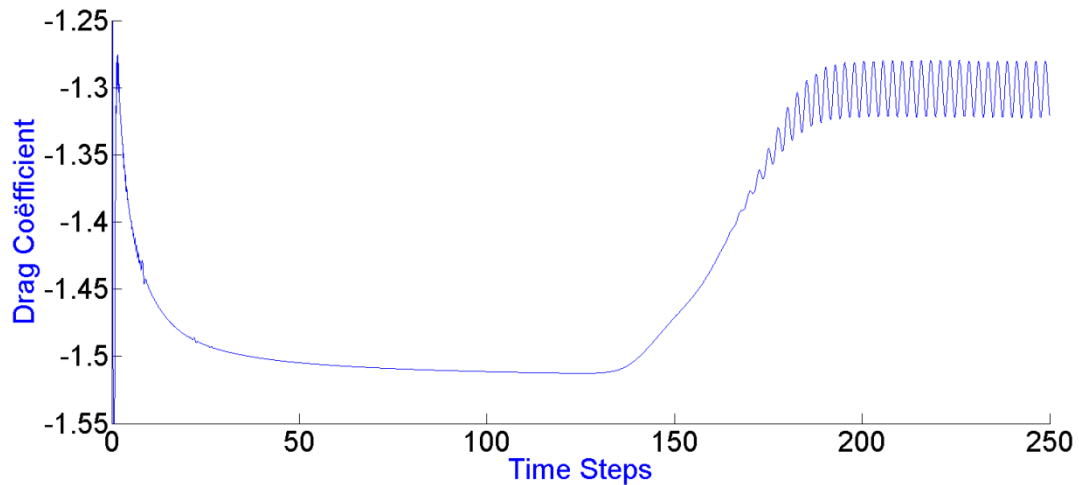


Figure 18 – Re= 200, T=1, Viscosity Constant

Figure 19 gives a close view of the fluctuation of the drag coefficient. The average value is -1.3 and the deviation is plus and minus 0.02. The shedding of one vortex causes one sine wave in the graph, and the frequency is based on the shedding of an upper and a lower vortex. From time step 225 to 250 there are 5 pairs of sinus waves and thus vortex pairs produced. This means the Strouhal number is $5/25 = 0.2$. This result corresponds to the values found in literature as shown in figure 3. The force on the cylinder works in the direction of the flow, the negative drag coefficients indicate the forces of the cylinder on the flow.

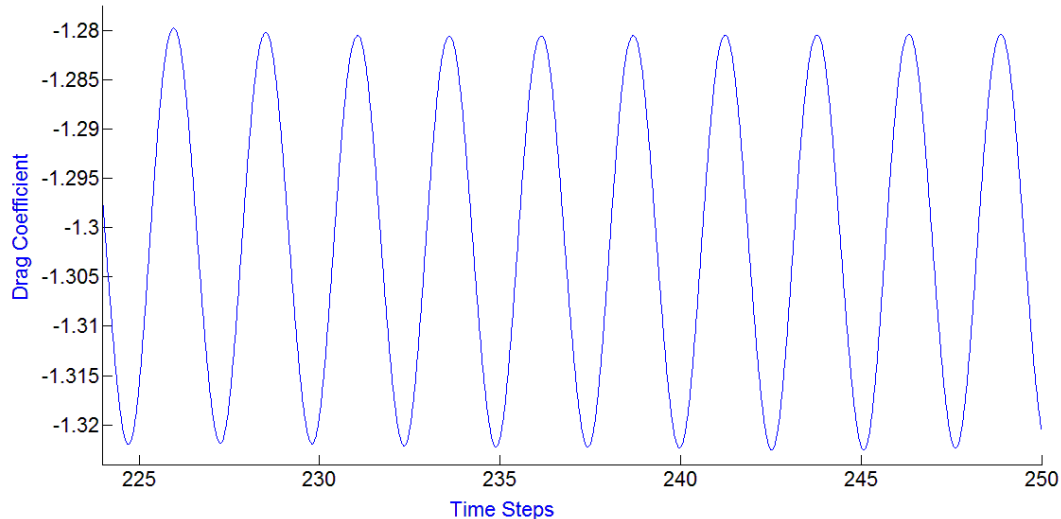


Figure 19 – Re=200, T=1, Viscosity Constant, Zoom

Reynolds number effect

The above benchmark shows how a Kármán vortex street develops in a flow with a Reynolds number of 200. For different Reynolds numbers, different results can be expected. The Reynolds number is varied around 200: Re= 100, 150, 250, 300, 400 and 500.

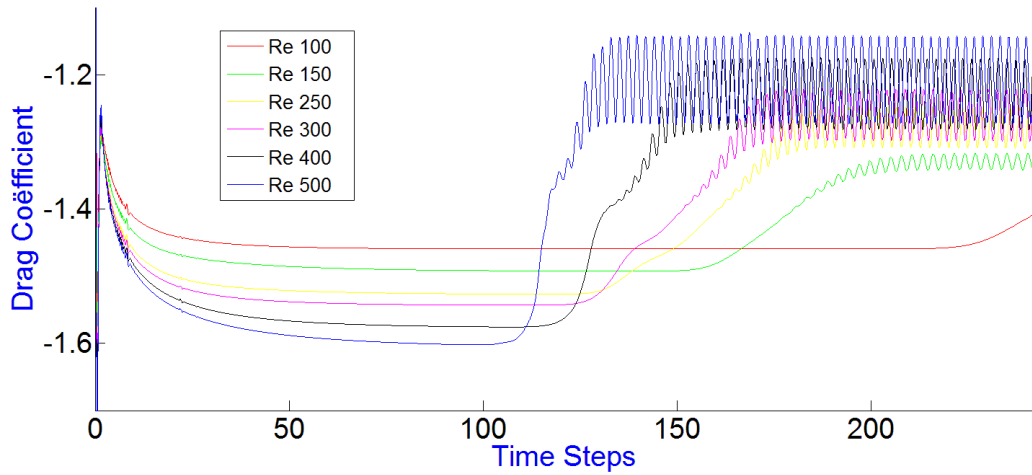


Figure 20 – Drag Coefficient versus Timestep, varying Reynolds number.

In figure 20 the drag coefficient is plotted as function of time for different Reynolds numbers. This graph clearly shows 4 differences between the solutions:

- The higher the Reynolds number, the lower the average drag coefficient. The average drag coefficient is determined when the Kármán street is fully developed. In figure 21 the Reynolds number is plotted against this drag coefficient. The difference between the lowest and highest Reynolds number, thus Re=150 and 500, is more than 5%.

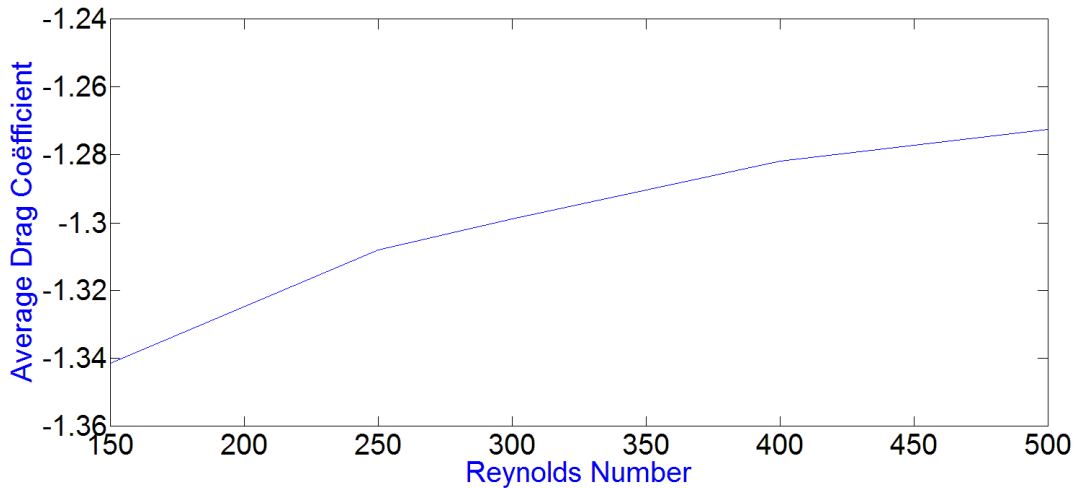


Figure 21 - Average Drag Coefficient versus Reynolds number

- The higher the Reynolds number, the larger is the fluctuation around the average value of the drag coefficient. The amplitude of the oscillation part of the drag coefficient is plotted in figure 22 against the Reynolds number.

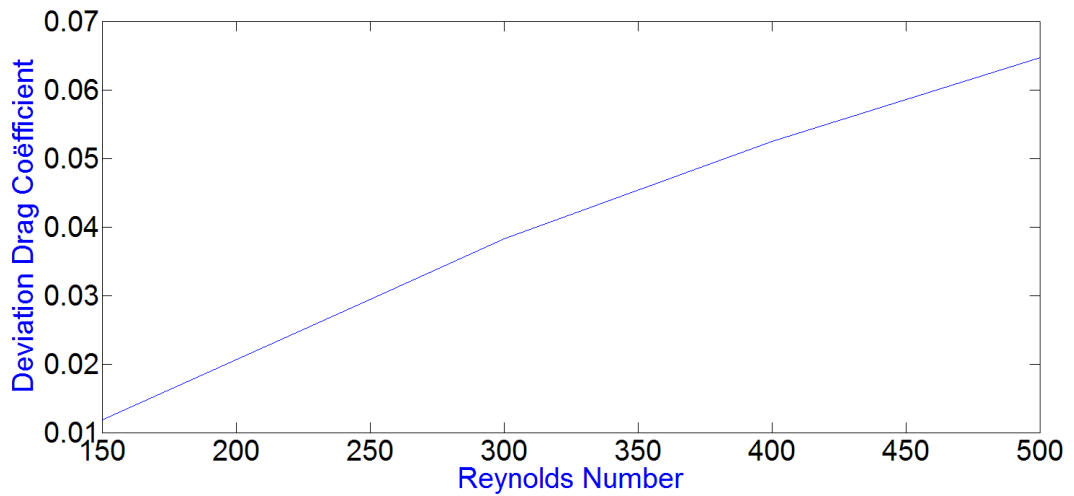


Figure 22 – Amplitude of oscillating part of drag versus Reynolds number

- The higher the Reynolds number the higher the Strouhal Number, this is shown in figure 23. For the range of Reynolds numbers considered, this result is in excellent agreement with figure 3, with the values of the Strouhal numbers as well as the trend in the graph, which is increasing from Reynolds 150 to 500. Otherwise stated, the calculations are in agreement with the literature.

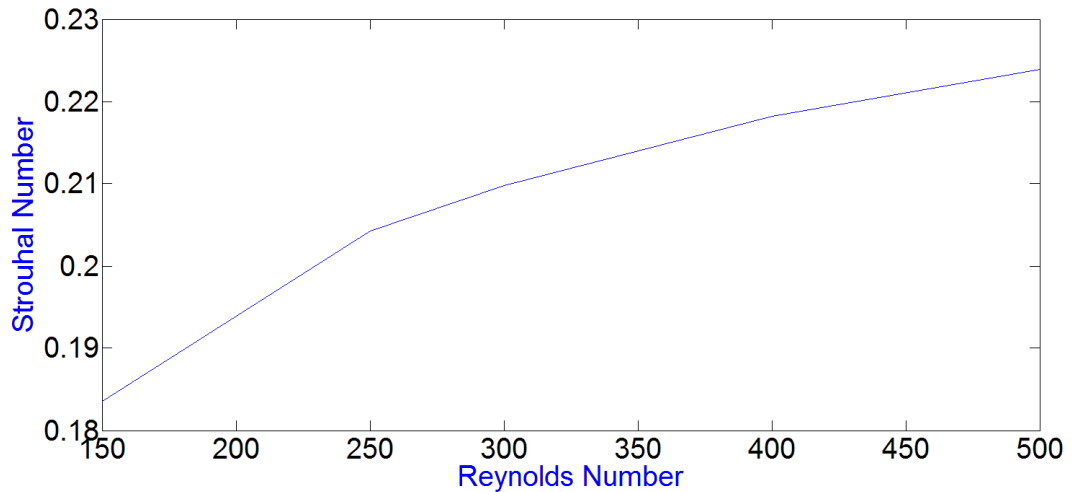


Figure 23 - Strouhal number versus Reynolds number

- The higher the Reynolds number, the sooner the Kármán vortex street will start developing. This is graphically presented in figure 24. In this thesis the start of this development is defined as the shift from a more or less steady drag coefficient, to a decrease of drag with time. For convenience, this is shown in figure 20 but the $Re=500$ case, here the steady drag coefficient of -1.6 decreases to a mean drag coefficient of -1.2 at timestep 110.

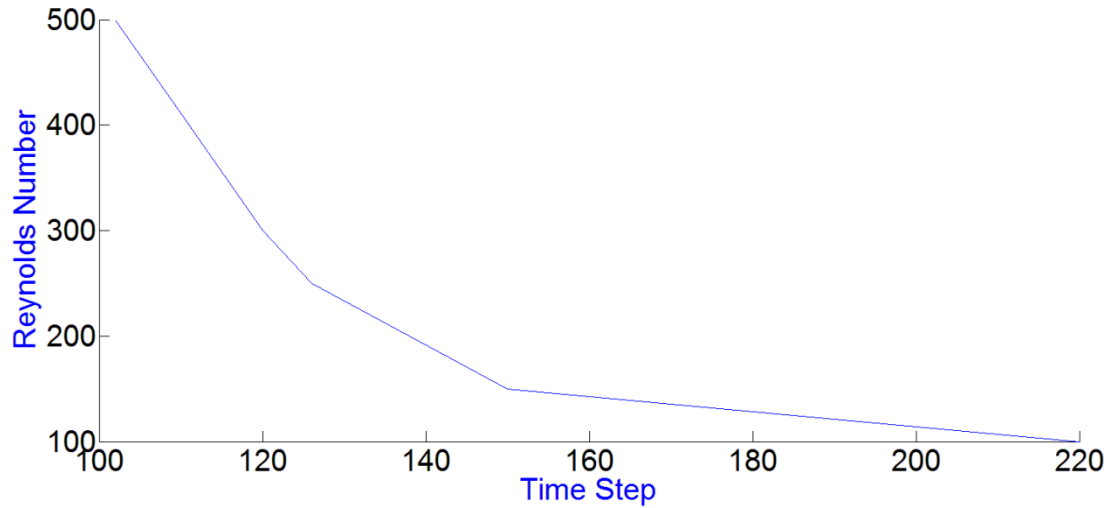


Figure 24 - Time at which wake starts to become oscillating versus Reynolds Number

Control of Flow by Heating of Cylinder

In the following we investigate the influence of heating and cooling the cylinder on the development of, the Kármán vortex street and the flow around the cylinder. First the case with a flow of air will be treated, followed by the case with water. The viscosity depends on temperature in both cases.

Air

The influence of heating the cylinder in a flow of air is started by increasing the temperature with 5%, 7% and 10% in comparison to the surrounding flow. The results of the four simulations, i.e. the four Kármán vortex street developments, are presented in figure 25. The differences are small but present.

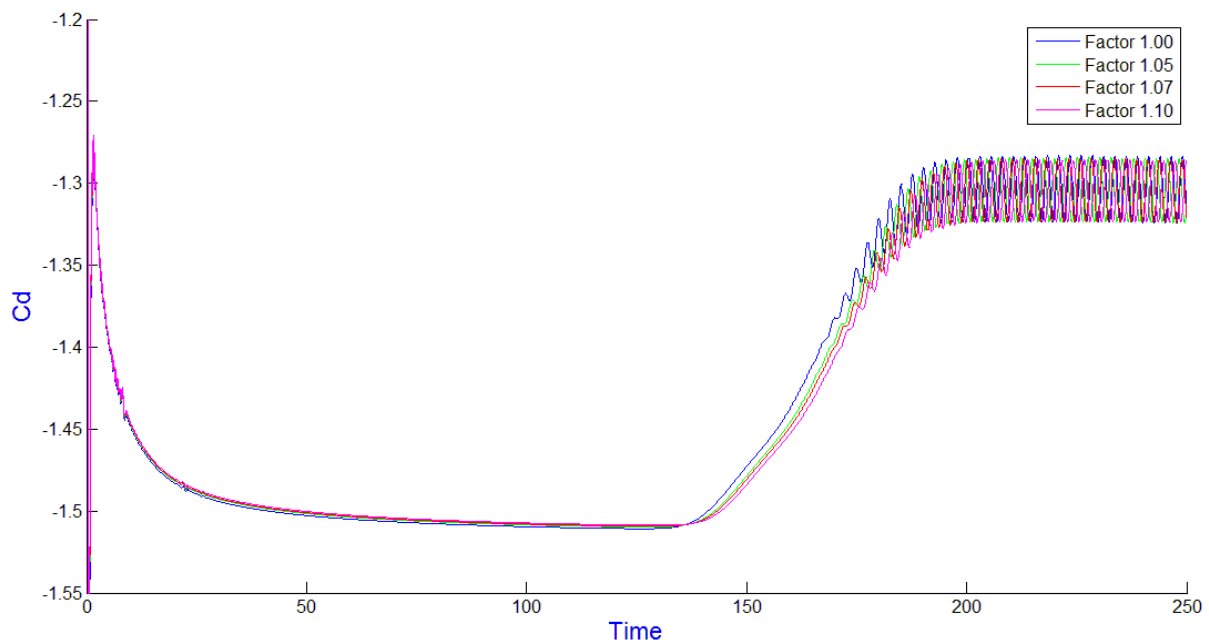


Figure 25 - Development Kármán vortex street for different cylinder temperatures. Fluid is air, $Re=200$.

Because the differences are small, figure 26 shows a close up of the moment the flow becomes oscillatory. It is clear that with increasing temperature of the cylinder, the moment the flow becomes oscillatory is postponed. This is in agreement with the theory as described in Chapter 1 paragraph 'Flow control', which states that with adding heat to the cylinder the formation of a Kármán vortex street can be postponed or, in the case of low Reynolds number flows, even be suppressed completely.

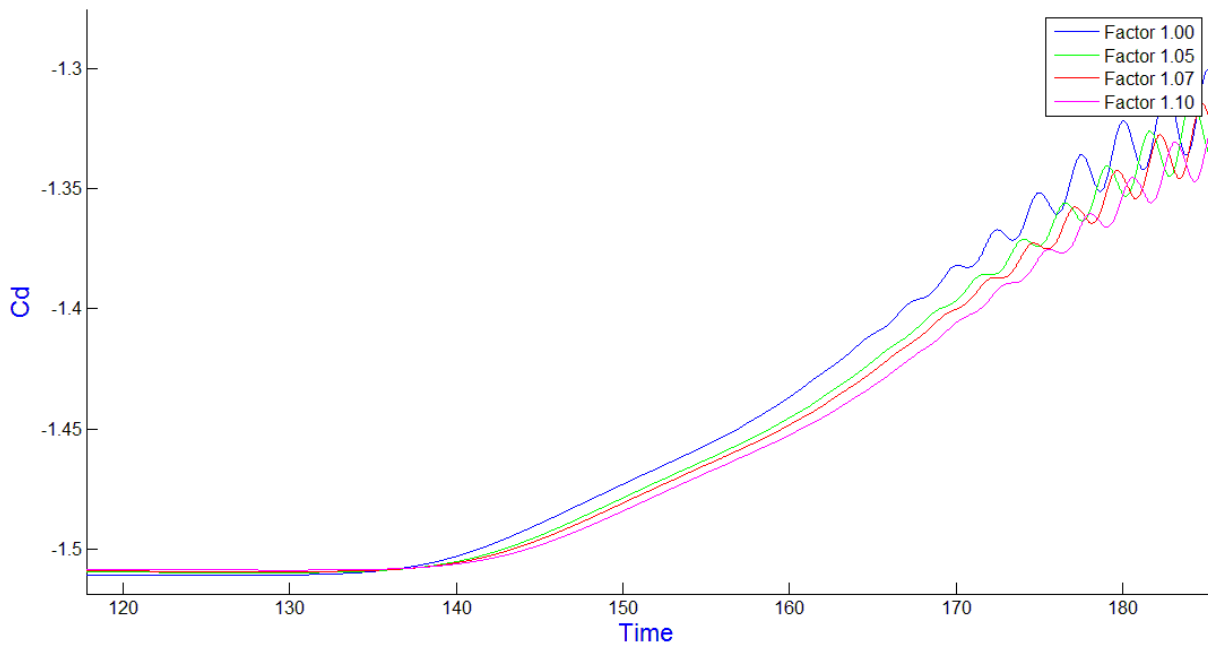


Figure 26 - Development Kármán vortex street for different cylinder temperatures, Zoom. Fluid is air, $Re=200$.

Now the range of the temperature factor is widened from 0.85 to 1.4. The calculations have been limited to a factor 1.4, because higher factors were not possible with the software used. The cooling is investigated to find out whether the effect of cooling is the reverse of that of heating.

The cylinder now is heated and cooled, the results are shown in figure 27. The red colored signal is the drag versus time for the cylinder that is heated with a factor 0.85 in comparison to the flow. The magenta colored plot is the case with heating factor 1.4. The plots in between are for factors 0.9, 0.95, 1, 1.15, 1.2, 1.25, 1.30 and 1.35, respectively.

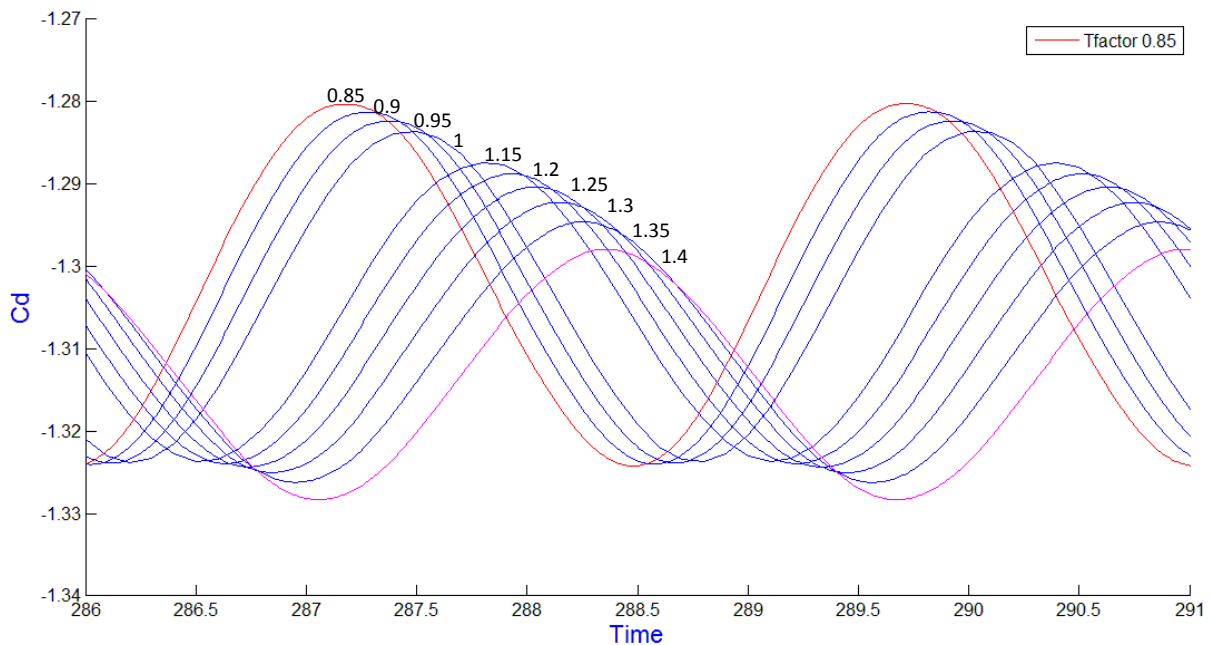


Figure 27 - Drag coefficient versus Time, Varying cylinder temperatures. Fluid is air, $Re=200$.

The results presented in figure 27 have been obtained by changing the temperature of the cylinder, following the flow condition that the flow is fully developed for $T=1$. When the flow is now simulated for more than 20 time steps, the Kármán vortex street and its properties are fully adjusted to the new cylinder temperature. It has been confirmed that there is no difference in comparison to the full simulations, starting directly with the cylinder at the given temperature.

From figure 27 can be seen what the influences are of changing the cylinder temperature.

- The average drag coefficient varies with the temperature of the cylinder. The change is presented in figure 28. Although there is a change, between the drag coefficient for the factor 0.85 and 1.4 this is only 0.81%, which is a negligible effect.

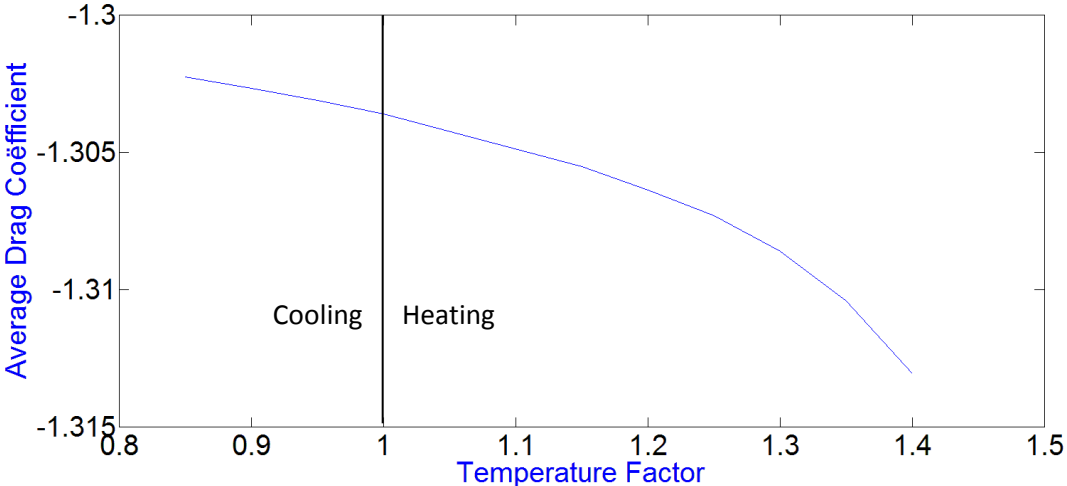


Figure 28 - Average drag coefficient versus Temperature Factor. Fluid is air, $Re=200$.

- The Strouhal number does also change with cylinder temperature. For higher temperatures the frequency becomes lower. For a temperature factor of 0.85 the frequency of the vortex shedding is $Sr=0.197$ and for a temperature factor of 1.4 it is $Sr=0.191$. Thus with a temperature difference of 65% the frequency change is not even 3%. This change is therefore also negligible.
- The higher the temperature factor, the larger is the fluctuation around the average value of the drag coefficient. The amplitude of the oscillating part of the drag coefficient, for a temperature of factor 0.85 and 1.4 is respectively 0.0219 and 0.015, respectively. Compared to the variation with respect to the Reynolds number case, figure 22, also this change is small and negligible.

The differences induced by heating and cooling of the cylinder, with the range considered, are hardly comparable to the differences induced by changing the Reynolds number of the flow. To compare these variations, quantifications are given in table 1.

| | difference between $Re\ 100\ \&\ 500$ | difference between Temp factor 0.85 & 1.4 |
|------------------------|---------------------------------------|---|
| Average Drag | >5% | 0.81% |
| Strouhal Number | 19% | <3% |
| Amplitude Oscillations | 0.012 & 0.065 | 0.015 & 0.0219 |

Tabel 1 - Quantification of Changes, Air

In general it can be stated that the differences induced by the heating and cooling of the cylinder, in the range considered, in a flow of air, are very small and all differences are practically negligible. In this scenario, for these flow specifications, the Kármán vortex street cannot be manipulated in a significant way.

Water

The following describes similar results for a cylinder in a flow of water. The study of the influence of the heating of the cylinder is started by increasing the temperature with 5%, 7% and 10% in comparison to the temperature of the surrounding flow. The results of the four simulations, i.e. the four Kármán street developments, are presented in figure 29. The differences are again small but clearly larger than the differences in the case of air.

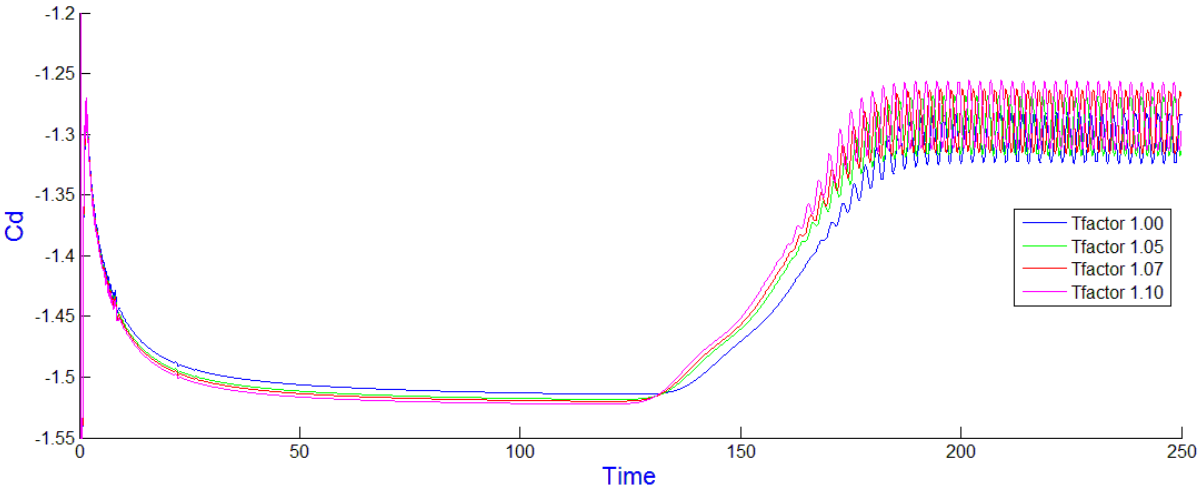


Figure 29 - Drag coefficient versus Time for varying cylinder wall temperatures. Fluid is water, Re=200.

To get a better view of the differences, figure 30 shows a close up of the moment the flow becomes oscillatory. It is clear that with increasing temperature of the cylinder, the moment the flow becomes oscillatory is earlier. This is the opposite behavior as seen in the case of air. This is again in agreement with the theory as described in Chapter 1 paragraph 'Flow control'.

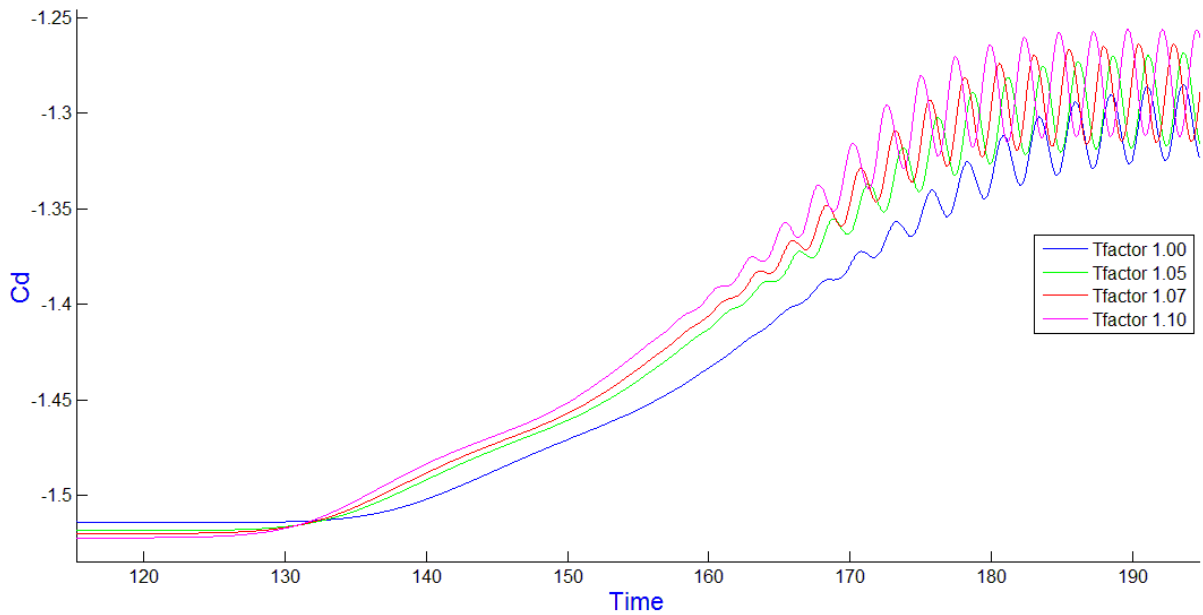


Figure 30 - Drag coefficient versus Time varying cylinder wall temperatures. Fluid is water, $Re=200$.

Figure 30 also makes clear that the drag coefficient is more sensitive to a change in temperature in case of water instead of air. When looking at figure 12 and 13, the plots of the viscosity of air and water versus temperature, we see this behavior confirmed. The viscosity of water is much more sensitive to temperature than that of air.

Because of the latter and the findings as described above the range of wall temperatures researched is taken from a factor 0.9 to 1.1 with steps of 0.02. We limited the factor to 1.1 because in the practical setup this is found as the maximum factor before side effects starts to play a significant role. The result are shown in figures 31 and 32. The temperature factors vary from 0.9 to 1.08 increasing with steps of 0.02.

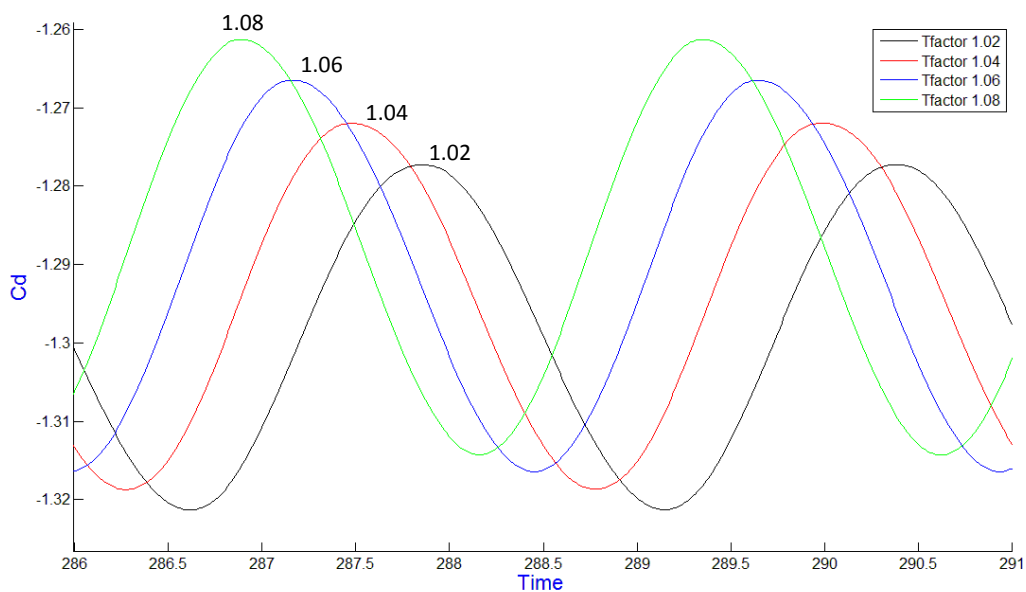


Figure 31 - Drag coefficient versus Time, Varying cylinder temperature: Heating. Fluid is water, $Re=200$.

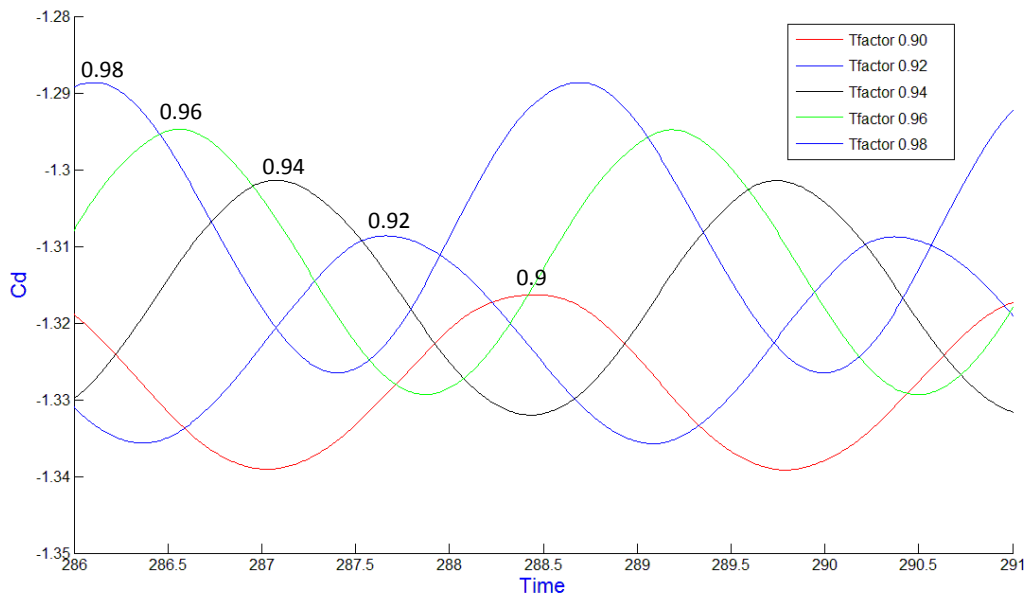


Figure 32 - Drag coefficient versus Time, Varying cylinder temperature: Cooling. Fluid is water, Re=200.

From these figures it can be seen what the influences are of varying the cylinder temperature.

- The average drag coefficient varies with the cylinder temperature, with an increasing cylinder temperature the average drag coefficient decreases. The change is presented in figure 33. The difference in drag between the two outer cases, so factor 0.9 and 1.08, is >3%. This is significant compared to the results for the variation obtained from changing the Reynolds number case, shown in figure 21.

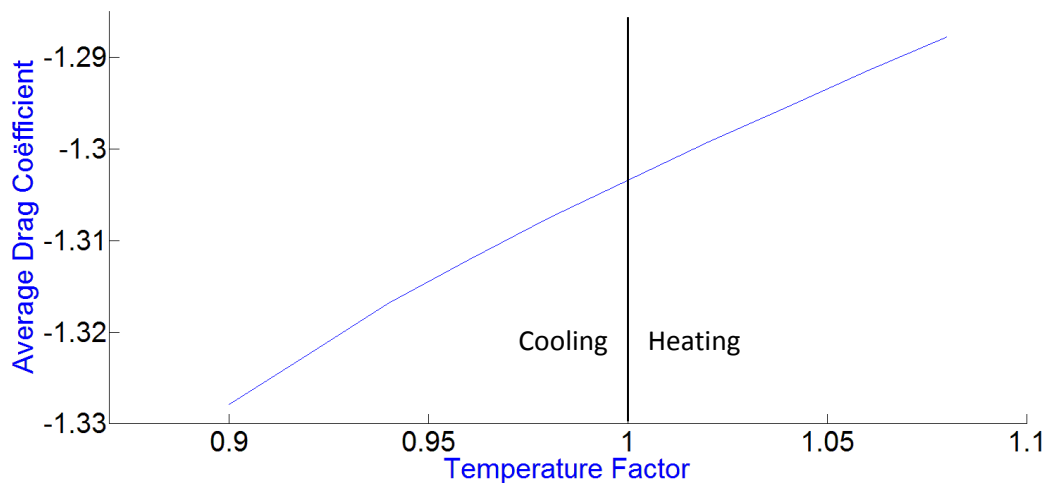


Figure 33 - Average drag coefficient versus Temperature Factor. Fluid is water, Re=200.

- The frequency, or Strouhal number, also changes with cylinder temperature. For higher Reynolds numbers the Strouhal number increases. In the case of water the difference is more significant than in the case of air. The result is plotted in figure 34. The difference between a temperature factor of 0.9 and 1.1 is an increase of almost 13%.

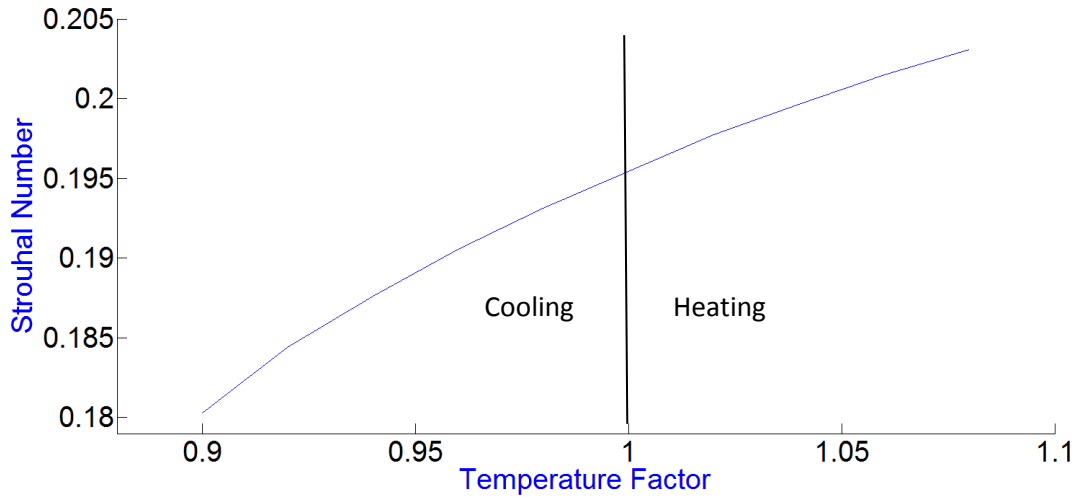


Figure 34 – Strouhal number versus Temperature Factor. Fluid is water, Re=200.

- The change in the amplitude of the oscillatory part of the drag coefficient is the largest change observed, see figure 35. When the cylinder is cooled with a factor 0.9 the drag varies with plus and minus 0.0114. In the case of heating the cylinder with a factor 1.08 this amplitude of the oscillatory part of the drag is increased to 0.0265.

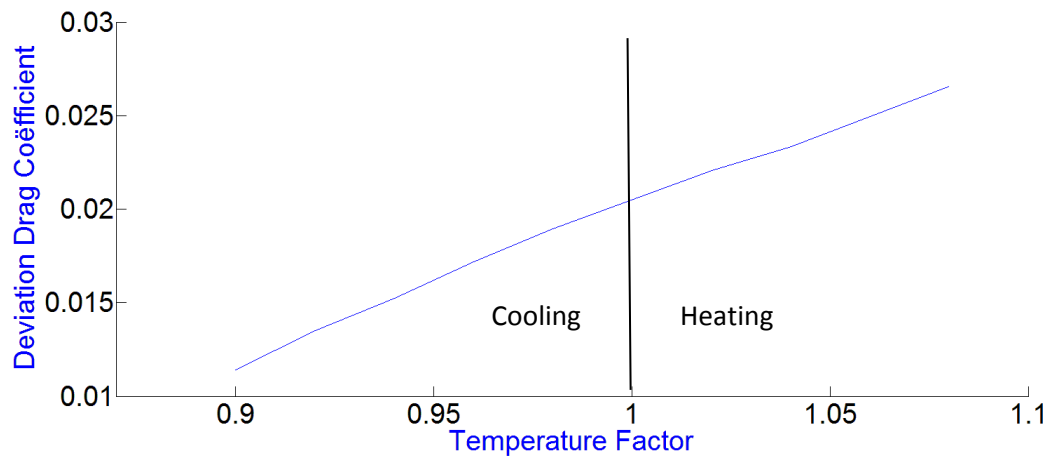


Figure 35 – Amplitude of oscillatory part of drag coefficient versus Temperature Factor. Fluid is water, Re=200.

In the range considered the differences associated with changing the Reynolds number of the flow are comparable to the differences associated with heating and cooling the cylinder. To compare these results, quantifications are given in table 2.

| | difference between Re 100 & 500 | difference between factor 0.9 & 1.08 |
|-----------------|---------------------------------|--------------------------------------|
| Average Drag | >5% | >3% |
| Strouhal Number | 19% | 13% |
| Amplitude | 0.012 & 0.065 | 0.0114 & 0.0265 |

Tabel 2 - Quantification of Variations

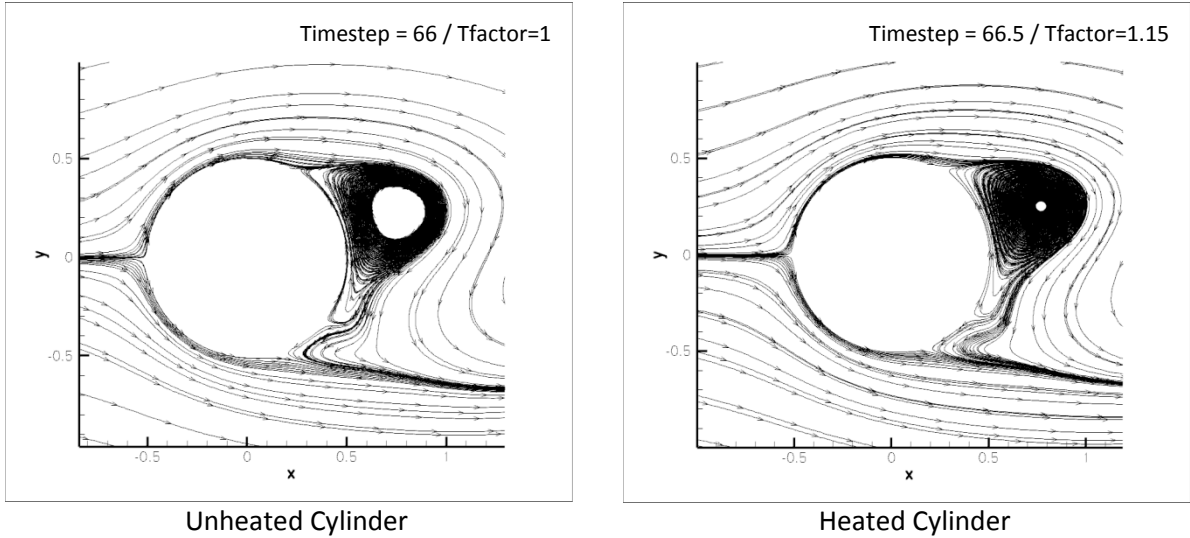
It is well known⁽²⁾ that for different Reynolds numbers, different wakes appear. As can be seen in table 2 all the variations, in C_d , St and oscillation amplitude, induced by changing the Reynolds number are also induced by changing the temperature of the cylinder.

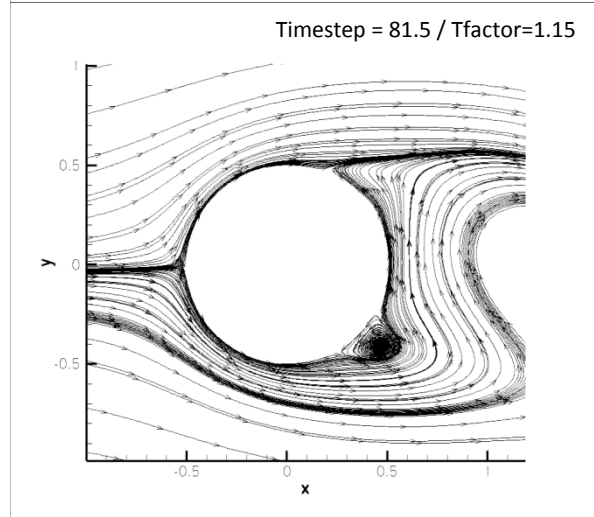
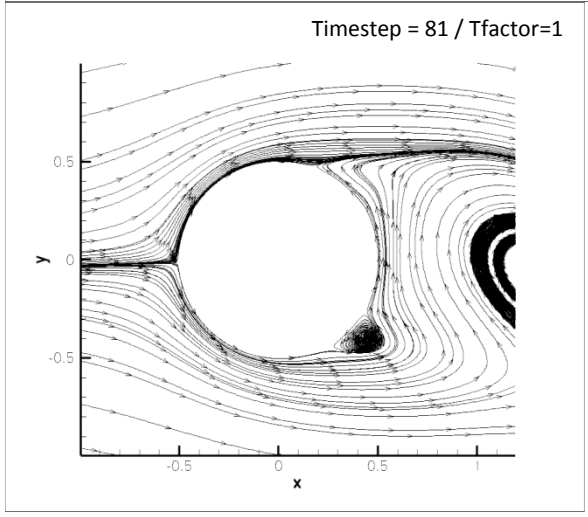
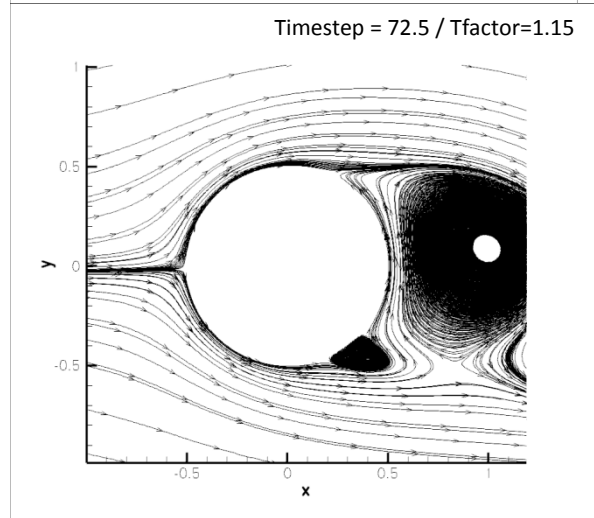
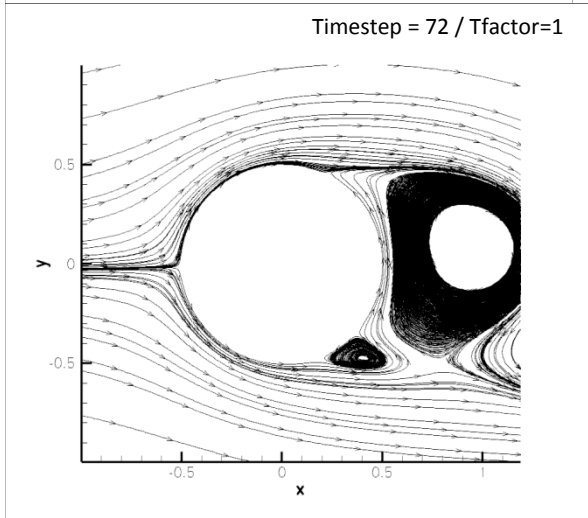
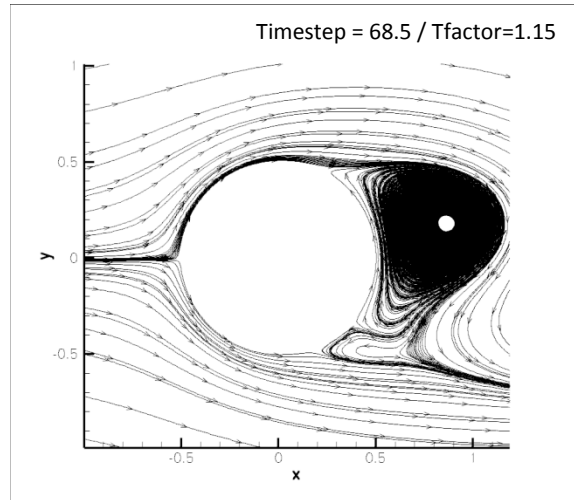
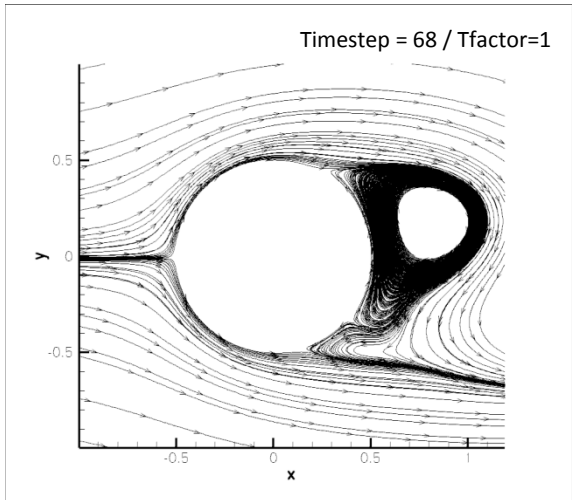
It can be concluded that the wake of a cylinder in a flow of water with Reynolds number 200 and Mach number 0.2 can be manipulated by changing the temperature of the cylinder. It appears that the effects of an increase of the temperature factor is comparable to the effects of an increase of the Reynolds number, thus the effective Reynolds number increases by heating the cylinder.

Case Air - Confirmed

In the case of air it appears that with variation of cylinder temperature only the boundary layer is affected. For a different temperature, the boundary layer has a different viscosity. The influences of the heated cylinder are too small to have an impact on the, development of, the Kármán vortex street.

We confirmed this presumption by comparing the case of an unheated cylinder, factor 1.0, with the case for which the cylinder is heated with a temperature factor of 1.15. Visualizing the flow with streamlines will show the effects. In figure 36 there are 5 snapshots for both cases, taken at the same moment in a shedding cycle.





Unheated Cylinder

Heated Cylinder

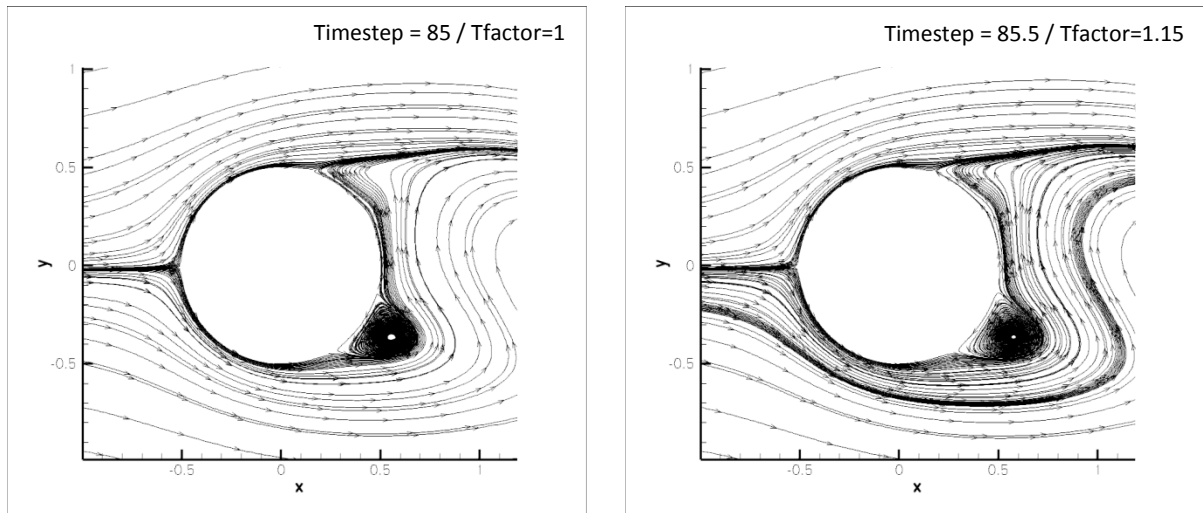


Figure 36 – Streamlines. Temperature factor 1 (left), Temperature factor 1.15 (right). Fluid is air, $Re=200$.

Figure 36 shows that the flows in the two cases are very similar. The points of separation are at the same point, the speed of the formation of the vortices is very much the same and the size of the vortices is about equal. It appears that the temperature increase has only influence on the laminar boundary layer and not on the point of separation of the boundary layer and the subsequent generation of the vortices or any other characteristic of the Kármán vortex street. Manipulating the flow of air by heating or cooling the cylinder is not possible in this case.

Future research for this case could be focused on the boundary layer and its changes. Due to time restrictions this report will not go into further details of the boundary layer. Due to the same reason, no comparison is made to the case of water.

Chapter 4 – Conclusions & Recommendations

Conclusions

In this research we have considered the effect of viscosity on the wake of a heated circular cylinder placed in flows of air and water. The Reynolds number is 200 and the Mach number is 0.2. In our study we used a DNS CFD method. The results provide insight needed for the practical setup at UCLA in a wider range of flows. Furthermore attention is paid to the possibilities to manipulate the wake by the heating and cooling the cylinder.

This Chapter is divided in two parts, the first part contains the conclusions of the performed CFD research. The last part is reserved for recommendations for future research.

As a benchmark case we investigated the differences of the wakes for varying Reynolds numbers. Four significant differences have been found: with increasing Reynolds numbers, the average drag decreases, the amplitude of the drag fluctuations increase, the Strouhal number increases and the development of the Kármán vortex street is provoked.

Similar results are found for a flow of water while heating the cylinder, even the order of magnitude of the changes are the same, see table 2. This suggests that heating the cylinder changes the effective Reynolds number. Thus the flow can be manipulated: by adding heat the formation of a Kármán vortex street in the wake is postponed, the opposite effect is obtained when the cylinder is cooled.

Similar calculations have been performed for a flow of air over a heated cylinder. In the range considered no significant changes have been discovered. This implies that the wake is not affected by the heating, this has been confirmed with a visualization study. Manipulation in this case is thus not possible.

The only difference between the case of the flow of water and that of air is the viscosity and its relation of temperature. Thus it can be concluded that the viscosity is of major influence on the wake which translates directly to the possibility of manipulating the flow.

Future Work

Future research could focus on the correlation between the temperature factor and the effective Reynolds number. To do so more calculations are necessary in, at least, the temperature factor region 0.9 – 1.1. Also research needs to be done to find out where other effects, in the case considered here secondary, like buoyancy, have a significant influence on the results.

With a better relation between heating and the effective Reynolds number, the practical setup can be used to verify a wide range of flows by changing the temperature of the cylinder as well as, for example, the speed of the flow.

Cited Literature

1. Zdravkovich, M. M.: Different modes of vortex shedding: an overview. J. Fluids and Structures, 10:427–437, 1996.
2. White, F. M.: Viscous Fluid Flow. New York, NY, McGraw-Hill, 1991.
3. Roshko, A.: Perspectives on bluff body aerodynamics. J. Wind Ind. Aerodyn. 49:7, 1993.
4. Williamson, C. H. K.: Vortex Dynamics in the cylinder wake. Annu. Rev. Fluid Mech., 28:477-539, 1996.
5. Dumouchell, F., Lecordier, J. C. and Paranthoën, P.: The effective Reynolds number of a heated cylinder, Int. J. Heat Mass Transfer, 41:1787-1794, 1998.
6. Ponta, F. L.: Vortex decay in the Kármán eddy street, Physics of Fluids, 22, 2010.
7. Lecordier, J. C., Browne, L. W. B. and Le Masson, S.: Control of vortex shedding by thermal effect at low Reynolds numbers, Exp. Thermal and Fluid Science, 21:227-237, 2000.
8. Yu, M.H. and Monkewitz, P.A.: The effect of nonuniform density on the absolute instability of two dimensional inertial jets and wakes, Phys. Fluids, 1175-1181, 1990.
9. Yang, X. and Zebib, A.: Absolute and convective instability of a cylinder wake, Phys. Fluids 1:689-696, 1989.
10. Varaprasad Patnaik, B. S., Aswatha Narayana, P. A. and Seetharamu, K. N.: Numerical simulation of vortex shedding past a circular cylinder under the influence of buoyancy, Heat and Mass Transfer, 42:3495-3507, 1999.
11. Kieft, R. N., Rindt, C. C. M. and van Steenhoven, A.A.: The wake behaviour behind a heated horizontal cylinder, Exp. Thermal and Fluid Science, 19:183-193, 1999.
12. Lecordier, J. C., Hamma, L., Paranthoen, P.: The control of vortex shedding behind heated circular cylinders at low Reynolds numbers, Exp. Fluids, 10:224-229, 1991.
13. Jacobs, G. B.: Numerical simulation of two-phase turbulent compressible flows with a multidomain spectral method. Doctoral dissertation, Univ. of Illionois at Chicago, 2003.
14. Kopriva, D.A. and Kolas, J.H.: A conservative staggered-grid Chebyshev multidomain method for compressible flows. J. Comp. Phys., 125:244-261, 1996.
15. Strouhal, V.: On one particular way of tone generation, Annals of Physics and Chemistry, 5:216-251, 1878.